Nano Today (2016) 11, 189—211

Available online at www.sciencedirect.com

ScienceDirect

journal homepage: www.elsevier.com/locate/nanotoday

REVIEW

Charge transfer and separation in photoexcited quantum dot-based systems

Kirill V. Vokhmintcev[a], Pavel S. Samokhvalov[a], Igor Nabiev[a,b,*]

[a] *Laboratory of Nano-Bioengineering, National Research Nuclear University MEPhI (Moscow Engineering Physics Institute), 31, Kashirskoe shosse, 115409 Moscow, Russian Federation*
[b] *Laboratoire de Recherche en Nanosciences, LRN — EA4682, Université de Reims Champagne-Ardenne, 51100 Reims, France*

Received 4 December 2015; received in revised form 15 February 2016; accepted 4 April 2016
Available online 27 April 2016

KEYWORDS
Nanocrystals;
Quantum dots;
Surface ligands;
Organic molecules;
Charge transfer;
Fluorescence;
Photocatalysis;
Solar cells;
Light-emitting diodes

Summary Colloidal quantum dots (QDs) are semiconductor nanocrystals which exhibit strong photoluminescence and have a variety of applications in modern nanotechnology. Specifically, QDs may serve as source of photoelectrical response to optical excitation, thus paving the way to development of novel optoelectronic and photovoltaic QD-based systems and devices. QD photoexcitation gives rise to excitons, electron—hole pairs which are bound by Coulomb forces and may dissociate in such a way that the charge carriers leave the nanoparticle and interact with the environment. The surface of inorganic QDs is always covered with organic ligands ensuring their colloidal stability during the synthesis and subsequent processing. The possibility to control the composition of the surface ligands is considered a promising way to modulate different parameters of charge formation and separation in nanoparticles, including the secondary pathways of charge transfer, rates of carrier generation, radiative or nonradiative electron—hole recombination, and some others.

The rates and directions of these processes strongly affect the fundamental photophysical properties of QDs, such as luminescence quantum yield, quenching, bleaching, blinking, and photostability; they also determine the applicability of nanocrystals to specific areas of photovoltaics, photocatalysis, and bioanalysis, as well as fabrication of light-emitting diodes (LEDs) and QD cellular automata (the transistorless computation paradigm).

Abbreviations: (P)ET, (photoinduced) electron transfer; (O)LED, (organic) light emitting diode; CB(E), conduction band (edge); CT, charge transfer; CV, cyclic voltammetry; EL, electroluminescence; ETL, electron transport layer; E_{vac}, vacuum level; FRET, Förster resonance energy transfer; HOMO, highest occupied molecular orbital; (P)HT, (photoinduced) hole transfer; HTL, hole transport layer; IPCE, incident photon to current conversion efficiency; LUMO, lowest unoccupied molecular orbital; MPA, mercaptopropionic acid; NHSs, nanoheterostructures; PEDOT:PSS, poly(3,4-ethylenedioxythiophene)-poly(styrenesulfonate); PL, photoluminescence; PV, photovoltaics; QD, quantum dot; TA, transient absorption; TOPO, trioctylphosphine oxide; UPS, ultraviolet photoelectron spectroscopy; VB(E), valence band (edge); XPS, X-ray photoelectron spectroscopy.

* Corresponding author at: Laboratoire de Recherche en Nanosciences, LRN — EA4682, Université de Reims Champagne-Ardenne, 51100 Reims, France. Tel.: +33 631259180.
E-mail address: igor.nabiev@gmail.com (I. Nabiev).

http://dx.doi.org/10.1016/j.nantod.2016.04.005

In this review we analyze recent advances in controlled charge generation, separation, and transfer in QD-based organic and inorganic systems, with a special emphasis on the role of the surface-stabilizing ligands in the transfer and separation of photogenerated charge carriers. The prospects of development of advanced QD-based photovoltaic and optoelectronic devices employing carefully selected surface ligands that improve the nanocrystal photophysical properties are analyzed in the ''Summary and outlook'' section.

Introduction

Nanostructured materials have been among the most promising and most intensely studied objects in the past two decades due to their unique properties, which are intermediate between those of bulk materials and molecular species. Quantum dots (QDs), one of the most attractive objects of nanotechnology [1], are semiconductor nanocrystals with the size ranging from 1 to 20 nm, which have some unique characteristics making them outstanding materials for LEDs [2,3], solar cells [4,5], photocatalysis [6,7], and biotechnology [8—10]. The size- and shape-controlled luminescence properties of QDs, high quantum yields and brightness of their photoluminescence, and the stability of QDs against photobleaching are underlain by the quantum confinement effect [11]. Furthermore, QDs have narrow luminescence bands with large Stokes shifts, which allows effective coupling of the emitted light to other fluorophores via Förster resonance energy transfer (FRET) and the use of QDs as light-harvesting antennae in hybrid materials [12,13] even in the two-photon mode [14]. QDs have large absorption cross-sections and, in contrast to organic fluorophores, may be excited by light with any wavelength corresponding to a photon energy higher than the energy of the first excitonic transition, which makes it possible to excite QDs of different sizes at a single wavelength and perform multiplexed detection of large series of analytes [15—18].

At present, colloidal synthesis that is conducted in liquid phase is the most powerful and versatile method for preparation of QDs. A distinctive feature of QDs obtained by colloidal methods is the presence of organic molecules (the surface ligands) on the surface of inorganic nanocrystals. The primary role of the surface ligands is stabilization of small inorganic clusters in a colloidal solution. In addition to this primary role, the ligands affect the nucleation and growth of QDs [14,19,20] by tuning the reactivities of nanocrystals [21,22] or their molecular building blocks [23], or even control the phase composition of nanocrystals [24,25]. Typically, the ligands are formed by conversion of precursors or are themselves components of the reaction medium. When the QD is formed in a colloidal solution, it represents a complex system consisting of inorganic core covered with a capping layer of organic surface ligands, often comprising multiple types of molecules. Modern techniques used for characterization of these complex ligand capping layers are reviewed in detail in Ref. [26].

Surface ligands can modify the optical properties of QDs, either causing shifts of the absorbance or photoluminescence spectra [27], quenching PL [28,29], or considerably enhancing it [30]. Because of their small size, QDs have a large surface-to-volume ratio; therefore, they actively interact with environment. The surface atoms of a QD may be undercoordinated due to the steric repulsion between ligand molecules located at the nanocrystal surface. The level of undercoordination can be reduced by passivation of the core surface using an inorganic shell [31]; however, the remaining unpassivated atoms have unbound orbitals that stick out from the QD surface and are thought to be the origin of charge-trapping states. Through these unpassivated sites, organic or inorganic molecules, semiconductor layers, or oxygen molecules can interact with QDs and affect their optical properties.

Excitation of a QD with the light whose photon energy is above the QD band gap results in the formation of an electrostatically bound electron—hole pair (exciton). Afterwards, the exciton may recombine and emit a photon with an energy beyond the band gap of the QD, recombine without emission of light, or dissociate into a pair of unbound charge carriers. Basically, these three processes determine the parameters of the QD photoluminescence, which, in turn, determines most QD applications. Exciton recombination parameters can be tuned by engineering of the QD inorganic structure: it is widely known that growing a shell of a high-band-gap material atop the photoluminescent core of the QD can dramatically increase the PL quantum yield [32], sometimes even to 100% [33—36]. However, a number of recent studies show that organic ligands, which are always present on the surface of colloidal QDs and are responsible for stabilization of colloidal solutions, can control the charge-carrier separation and transfer processes [37—40].

According to the Marcus theory [41], the driving force of the charge carrier transfer is the difference between the energy levels of the charge donor and acceptor (Fig. 1). Therefore, there are two ways to tune the driving force of charge transfer. The first way is to modify the positions of the QD band edges by changing the size of the QD [42]; the second one is to change the highest occupied molecular orbital (HOMO) or the lowest unoccupied molecular orbital

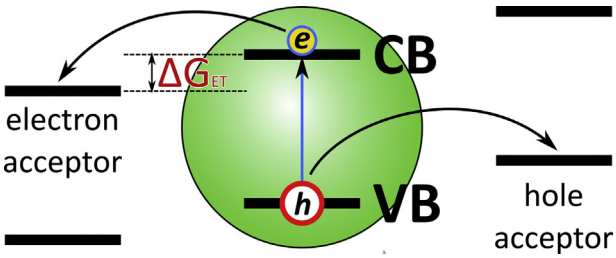

Figure 1 Schematic representation of photoinduced charge transfer between a quantum dot and charge acceptors. CB, conduction band; VB, valence band.

Table 1 Band energy levels in quantum dots, shells, and bulk materials.

Type	VBE[a]	CBE[a]	Methods and comments	Ref.
QD cores				
CdSe	−5.58 to −5.35	−2.92 to −3.38	2.1−6.4 nm, size-dependent band levels determined using photoelectron spectroscopy in air (PESA) and optical band gaps, several ligand types	[44]
CdSe	−5.55 to −5.25	–	2.1−3.7 nm, aromatic ligand dependence, size dependence, differential pulse voltammetry, density functional theory (DFT) calculations	[45]
CdSe	−5.74 to −5.59	−3.51 to −3.62	3−6.5 nm, cyclic voltammetry (CV) and optical measurements, TOPO as surface ligand	[46]
CdSe	−5.68 to −5.39	−2.83 to −3.20	1.9−3.6 nm, CV, TOPO as surface ligand	[47]
CdSe	−6.5 to −6.1[b]	–	3.6 and 6 nm, ultraviolet photoelectron spectroscopy (UPS), ionization potentials (IP) are given, ligand dependence and ligand-stripped QDs	[48]
CdSe	−6.68 to −4.78[b]	−1.11 to −4.71[b]	DFT calculation, $Cd_{33}X_{33}$, X = Se, Te, ligand and environment dependence, vertical and adiabatic values, IP and electron affinity (EA) values	[49]
CdSe	−5.59 to −5.47	−3.49 to −3.02	CdSe dot, rod, and tetrapod morphologies are compared, indirect optical measurement using the dopant approach	[50]
CdTe	−5.01 to −4.90	−2.51 to −3.09	2.3−5.6 nm	[44]
CdTe	−6.82 to −4.53	−1.01 to −4.64	DFT calculations	[49]
CdTe	−6.02 to −5.39	−3.54 to −3.61	2.4−4.7 nm, CV and DFT	[51]
ZnSe	−5.64 to −5.55	−2.32 to −2.62	2.6−4.6 nm	[50]
ZnO	–	−3.66 to −3.86	4.4−8.6 nm, CV, optical, Stark effect values measured relative to NHE	[52]
PbS	−5.01 to −4.87	−3.52 to −4.22	2.8−8.5 nm	[44]
PbS	−5.13	−4.54	9.8 nm nanocrystals, oleate capping, XPS	[53]
PbSe	−5.01 to −4.85	−3.68 to −4.26	2.1−8.3 nm	[44]
InAs	−4.85 to −4.7	–	<2−4.4 nm, CV, ligand dependence	[54]
InP	−5.18 to −5.10	−2.48 to −3.25	1.4−4.5 nm	[50]
$CuInS_2$	−5.76 to −5.73	−3.65 to −3.87	2.5−4, CV	[55]
QD shells				
ZnS	−6.09	−2.02 to −2.27	DFT calculation, slabs, 7−11 atomic layer thick (1.1−2.3 nm) and bulk data, zinc blende phase	[56]
ZnSe	−5.70	−2.40 to −2.83	’’	[56]
ZnTe	−5.18	−2.39 to −2.79	’’	[56]
CdS	−6.00	−3.04 to −3.42	’’	[56]
CdSe	−5.70	−3.34 to −3.88	’’	[56]
CdTe	−5.28	−3.18 to −3.68	’’	[56]
InP/ZnS	−5.30 to −5.12	−2.55 to −3.14	Shell thickness dependence, indirect optical measurement using the dopant approach	[50]
InP/ZnSe	−5.32 to −5.12	−2.57 to −3.20	Shell thickness dependence, indirect optical measurement using the dopant approach	[50]
Bulk materials				
ZnSe	–	−4.09[b]	EA measurement	[57]
ZnTe	–	−3.53[b]	’’	[57]
CdS	–	−4.79[b]	’’	[57]
CdSe	–	−4.95[b]	’’	[57]
CdTe	–	−4.28[b]	’’	[57]
CdSe	−5.24	−3.5	Indirect optical measurement using the dopant approach	[50]
CdO	–	−4.514[b]	EA also measured for F-doped films, measurements from optical data	[58]
CdO	−5.4	–	UPS and X-ray photoelectron spectroscopy (XPS), n-type doping with In or Y	[59]

Table 1 (*Continued*)

Type	VBE[a]	CBE[a]	Methods and comments	Ref.
$CH_3NH_3PbI_3$	−5.75[b]	–	Thin film on different substrates, XPS and UPS	[60]
$CH_3NH_3PbI_3$	−5.4	−3.9	DFT calculations	[61]
$CH_3NH_3PbBr_{3-x}Cl_x$	−6.83 to −5.77	−3.23 to −4.34	UPS, alloyed materials with $x = 0$, 0.6, 1.2, 1.8, 2.4, 3, work functions	[62]

[a] VBE = valence band edge, CBE = conduction band edge, the values relative to the vacuum level are shown, recalculated by us where necessary.
[b] Ionization potential (IP) or electron affinity (EA) values.

(LUMO) energy level [43] of the ligand or probe molecule by selecting the proper substance. Since the energy structure of the QD—ligand system governs the direction and type of intrinsic charge transfer, it is of utmost importance to know the relative and absolute QD band levels and the positions of the HOMO and LUMO of organic molecules (Table 1). We have attempted to summarize the available experimental and theoretical data on the energetics of the common types of QDs and bulk semiconductor materials. These data may be helpful for the reader in sketching the energy diagram of the QD studied.

The data shown in Table 1 may seem scattered at first glance, yet a number of authors believe that the ligands make a sufficient contribution to the band energies of QDs; this assumption has been confirmed for experimentally determined values [44,45] and theoretical predictions [49]. Theoretical calculations show how ligands affect the orbital energies of the $Cd_{33}Se_{33}$ cluster and how the loss of a single ligand can considerably change the energy structure of a QD, forming trap states located within the band gap [63]. Furthermore, the differences between the VBE and CBE values shown in Table 1 may result from the method of study and measurement conditions; it could hardly have been expected that the values obtained using UPS or XPS in high vacuum would coincide with those obtained by the CV method in a solution. In several publications, experimental data on band alignment in solid films [64,65], QD thin films [66—68], or core/shell systems [69] are presented that could be used for further analysis of the energy diagrams of QDs and QD-based systems. Numerous data on the ionization potentials, electron affinities, and the energies of frontier orbitals of organic compounds have been published [70—73], some of them available at the Internet [74]; the reader is referred to these sources to find the necessary information about energy levels of surface ligands or other organic molecules. However, it should be noted that, upon oriented adsorption of the ligand onto the polarized surface of QDs, these energy levels may vary considerably, which results in hybridized QD—ligand molecular orbitals [49,75].

Electron and hole transfer in quantum dot—ligand systems

If the energy of the ligand LUMO is lower than or equal to the edge of the conduction band (CB) of the QD core, the transfer of an electron from the inorganic part of the QD to the ligand molecule can occur. Since common QD surface ligands, such as amines, phosphine oxides, thiols, and phosphonic and carboxylic acid residues, are typically non-absorbing in the visible spectral range, different types of compounds, such as ethylene blue [76,77], Rhodamine B (RhB) [78,79], F27 [80], anthraquinone dyes [81]; viologen derivatives [77,82—86], 1,4-benzoquinone [87,88], organometallic complexes of transition metals [89—93], functionalized fullerenes [42,94—96], supramolecular assemblies [97], carbon nanotubes [98], etc. have become important classes of probe molecules for studying charge transfer on the surface of QDs by optical spectroscopy methods. These compounds are known to exhibit well-resolved optical transitions, which differ in reduced and oxidized states, and have large molar extinction coefficients; therefore, a few adsorbed molecules are enough to study charge transfer (Fig. 2).

Transient absorption (TA) spectroscopy has proven itself as the most powerful method for studying the kinetics of electron transfer. Prolonged excitation of QDs leads to population of the QD conduction band with electrons and the resultant bleach of excitonic transitions in the absorption spectra of QDs. Transfer of these high-energy electrons to the organic molecules on the QD surface leads to absorption bleach recovery, which can be detected and traced using TA (Fig. 2c—e).

Electron transfer: general principles and influence of ligand redox potential

The study by Boulesbaa et al. [79] represents a good example of the analysis of electron transfer kinetics using TA spectroscopy. There, electron transfer in the CdSe—RhB complex and ''bare'' oleic acid-capped CdSe nanocrystals was studied. The CdSe—RhB complex was obtained by adding RhB to a CdSe nanocrystal solution in heptane and subsequent sonication and filtration of the solution to remove undissolved RhB molecules. Since RhB is insoluble in heptane, all dye molecules that are present in the filtered solution were believed to be bound to CdSe QDs. Bare QDs capped with oleic acid were excited with pulsed laser radiation at 400 nm (pulses of 150 fs, 2.5 mJ/pulse). Transient absorption spectra show that exciton bleach recovers by ~15% within the first 10 ps; for the next 1 ns, the bleach intensity remained practically unchanged, which meant that, during the first nanosecond, most excited electrons were settled at the 1S level of the CdSe QD. The fast bleach recovery during the initial several picoseconds is attributed to multiple exciton generation [99] and fast exciton—exciton annihilation [100]. In the presence of RhB on the surface of QDs, the

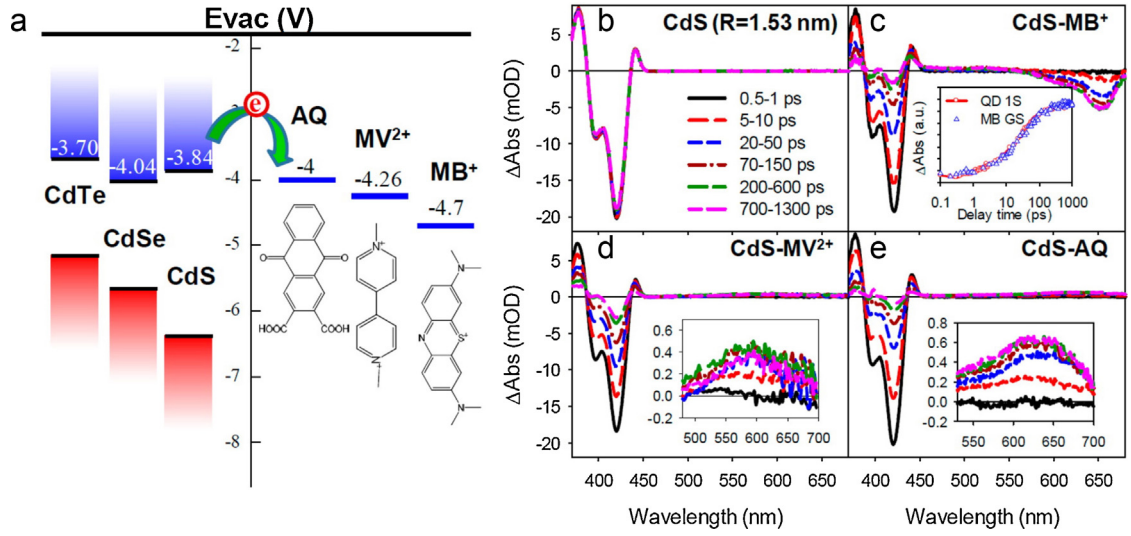

Figure 2 Schematic diagram of bulk conduction band edge positions of quantum dots and reduction potentials of acceptor molecules (vs vacuum) (a), transient absorption spectra of bare quantum dot (b), CdS—methylene blue (MB^+) complexes (c), CdS—methyl viologen (MV^{2+}) complexes (d), and CdS—anthraquinone complexes (AQ) (e). E_{vac} — vacuum level.
Reprinted with permission from [77]. Copyrights 2014 American Chemical Society.

authors observed bleach recovery of the CdSe—RhB complex at rates several times higher than in the absence of RhB. The transfer of electron to the adsorbed RhB leads to the formation of a charge-separated state between the CdSe QD and RhB molecule. It was also found that these charge-separated states are long-lived (with an average lifetime of 1 μs), and the dependence of the QD absorbance quenching kinetics on the number of adsorbates can be approximated by a kinetic model that assumes a Poisson distribution of adsorbate molecules on the surface of QDs.

On the other hand, the transfer of electron from a QD to a ligand or acceptor molecule may result in population of the LUMO of the adsorbed molecule with electrons, which, in turn, leads to bleach of ligand or acceptor absorption. Study of the bleach kinetics of the organic ligand is another way of investigation of electron transfer in the QD—ligand system. This approach has been applied to the complex of CdS with RhB dye [78]. The CdS—RhB complex was chosen because of its well-separated spectral signatures. The sample preparation procedure and parameters of the excitation were the same as in Ref. [101]. Here, the TA spectra contained two distinctive features: the bleach of the RhB ground state at 545 nm and an absorption band with a peak at ~425 nm. It has been shown that these features have similar kinetics, which indicates that the conversion of the ground-state RhB molecules into a new species absorbing at 425 nm occurs. The absorption band at ~425 nm is attributed to the formation of one electron-reduced RhB molecule, whose absorption band has been reported to be at ~420 nm. These results suggest that excitons in CdS QDs dissociate upon excitation, and an electron migrates from the CB of CdS to the unoccupied orbitals of RhB, forming a reduced RhB molecule. Therefore, the main characteristic of the electron transfer process is reduction of the ligand, which has been observed in numerous studies [42,76,82,90,102].

The mechanism of electron transfer between 1,4-benzoquinone (BQ) and PbS QDs coated with oleic acid was investigated using the TA spectroscopy by Knowles and colleagues [88]. Transient absorption measurements showed that this system had different electron transfer kinetics on the picosecond and microsecond scales. It was suggested that the reason for this phenomenon is that two different mechanisms of electron transfer operated on different time scales. The picosecond electron transfer was attributed to the transfer of electron to benzoquinone molecules adsorbed directly on the surface of PbS QDs. Regarding the microsecond process, there are two possible ways of electron transfer: (i) photoinduced electron transfer (PET) may occur upon photoexcitation via tunneling of the electron through the oleate ligand shell to benzoquinone molecules located within the shell, or (ii) benzoquinone molecules diffusing in the solution may collide with photoexcited QDs, some of these collisions resulting in PET. If the slow electron transfer were to occur via mechanism (i), multiple charge separation rate constants would be found due to the uniform distribution of benzoquinone molecules within the ligand shell over a range of distances from the surface of the QD (up to 19 Å). Hence, in order to obtain the experimentally observed charge separation rates, the donor—acceptor distances for the QD—BQ systems should have been less than 1—2 Å. However, it is unlikely that benzoquinone molecules randomly distributed within the QD ligand shell occupied such a narrow range of distances from the QD surface. Therefore, the collision mediated mechanism (ii) was found to be the most probable way of electron transfer between PbS QDs and BQ on the microsecond scale. Electron transfer is a multivariable process, and its rate depends on many parameters. A QD solution is an ensemble of nanoparticles, and experimenters actually deal with the statistical parameters of the ensemble. There are two general approaches to studying such systems. The first one is to study the whole system, with its external parameters assumed to be quasi-static. The second approach is to consider the charge separation and transfer processes for each QD individually; this approach

allows one to determine the distribution of adsorbed ligand molecules over the QD, which has been shown to influence the rate of electron transfer [42,92,97,103–106].

According to Morris-Cohen et al. [82], not all of the adsorbed ligand molecules are involved in electron transfer; a ligand molecule should be in the PET-active configuration for electron transfer to occur. The authors suggested a new method for determination of the number of PET-active ligand molecules per quantum dot (parameter noted as λ), the ligand adsorption constant K_a, and the intrinsic rate constant for PET $k_{cs,int}$ (on the basis of the observed PET rate $k_{cs,obs}$) from the kinetics of bleach recovery in the system consisting of CdSe QDs. The proposed method is based on the observation earlier [78,96]:

$$k_{cs,obs} = nk_{cs,\text{int}}, \tag{1}$$

where n is the number of ligands adsorbed on any single QD in the ensemble ($\lambda = \langle n \rangle$). Eq. (1) shows that the value of λ should be known to determine the intrinsic rate constant for PET ($k_{cs,int}$). It has been found that, in the case of non-interacting ligands, the number of adsorbed ligands per QD follows the Poisson distribution [107,108], and the probability of finding a QD with n adsorbed ligands, $p(n,\lambda)$, can be calculated as:

$$p(n,\lambda) = \frac{\lambda^n}{n!}e^{-\lambda} \tag{2}$$

The value of $p(n,\lambda)$ can be easily determined from the ground-state bleach recovery experiments. K_a can be estimated using the Langmuir adsorption isotherm after the conversion of λ into $\theta = \lambda / n_{sites}$:

$$\theta = \theta_{\max}\frac{Ka * [V^{2+}]_{free}}{1 + Ka * [V^{2+}]_{free}} \tag{3}$$

Song et al. [96] proposed a model describing electron transfer in the QD–ligand system with a dynamic distribution of the number of ligand molecules per QD. In this case, ensemble-average techniques, such as fluorescence decay and transient absorption spectroscopy, are unsuitable, since the composition of the system varies with time. The most effective method for studying such systems is single particle/molecule fluorescence spectroscopy. Single and ensemble-averaged QD fluorescence decay kinetics were measured using a scanning confocal microscope. Three samples of CdSe/CdS/CdZnS/ZnS core/graded alloy shell QDs with different average quantities of an adsorbed fullerene derivative were investigated using single particle fluorescence spectroscopy. It was supposed that, in the QD–C60 complex, electron transfer from the QD to fullerene was an additional pathway for fluorescence decay characterized by time-dependent rate constant $k_{ET(t)}$. It was also suggested that the intrinsic exciton decay, which was characterized by the average rate k_0 in the absence of the fullerene ligands, was not affected by electron transfer. It was shown that the growth of the electron transfer rate due to an increase in the amount of the ligand led to an increase in its standard deviation. The amplitude of the electron transfer rate and its standard deviation fit the Poisson distribution. This finding suggests that the distribution patterns of these parameters are determined by the heterogeneity of the number of ligands per QD.

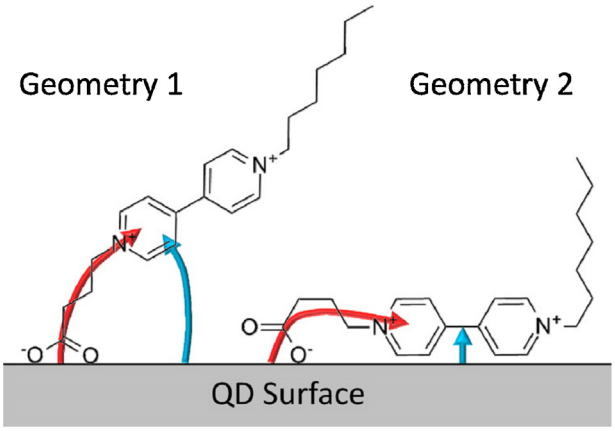

Figure 3 Schematic diagram of two possible adsorption geometries of asymmetric viologen ligands and two possible photoinduced electron transfer (PET) pathways.
Reprinted with permission from [85]. Copyrights 2012 American Chemical Society.

Influence of ligand adsorption geometry on electron transfer

In order to clarify the mechanism of electron transfer in the QD–ligand system, the role of the ligand adsorption geometry should be determined. The geometry of the viologen absorption was investigated by Morris-Cohen et al. [85]. In this paper, viologens with different numbers of carbon atoms in the alkyl chain between the surface-binding carboxyl group and the bipyridinium moiety were used (Fig. 3). Two possible mechanisms of electron transfer from CdS QDs to viologens with different amounts of methylene groups between the bipyridinium core and the linking group were suggested. The first, so-called ''through-bond'' mechanism (Fig. 3, geometry 1, red arrow) is the transfer of an electron from the QD to the bipyridinium core through the alkylcarboxylate group. The second, ''through-space'' mechanism (Fig. 3, geometry 1, blue arrow), occurs only through the orbitals of QDs and the bipyridinium core not involved in chemical bonding. If the observed electron transfer took place according to the ''through-bond'' mechanism, this would lead to a difference in the rates of electron transfer between methyl viologen and other viologens, the rate being dependent on the number of carbon atoms in the alkylcarboxylate group. However, transient absorption studies showed that the rate of the bleach recovery did not depend on the number of carbon atoms in this chain; hence, electrons were actually transferred via the ''through-space'' mechanism (blue arrow). These authors also mentioned two possible orientations of the adsorbed viologen molecules [85] (Fig. 3, geometries 1 and 2). In the case of geometry 1, the electrons would have to travel over a distance that directly depended on the number of carbon atoms, which would be reflected in the dependence of the electron transfer rate on the length of the alkyl chain. Since this was not observed, the authors suggested that the bipyridinium cores of viologens were physisorbed directly onto the surface of QDs.

Influence of ligand length on electron transfer

In order to investigate the influence of the distance between the QD and the electron acceptor on the rate of electron transfer, the authors of Ref. [84] have placed CdSe QDs with HS—$(CH_2)_n$—COOH ($n = 1, 2, 5, 7, 10$, or 15) as a native ligand into a polyviologen matrix. Here, in contrast to isolated viologen molecules, the acceptor moieties do not contact QDs directly and cannot be in the PET-active configuration. The rate of PET to the polyviologen was investigated with the use of transient absorption spectroscopy, where the non-redox-active polycation poly(diallyldimethylammonium) (PDDA) was used for comparative experiments. In the case of QDs coated with mercaptocarboxylic acid ligands with the number of methylene groups ranging from 1 to 7 dispersed in polyviologen matrix, very fast PET was observed. The PET rate was significantly higher than that between non-redox-active PDDA and QDs. In the case of long-chain ligands with $n = 10$—15, the PET rate was significantly decreased compared to QDs with short ligands. It was assumed that the difference between the PET rates for the C1—C7 and C10—C15 ligands was caused by transition of the ligand layer from a disordered liquid-like state to a highly ordered compact monolayer state with increasing ligand length. Similar phase transitions were observed for other nanoparticles with ligand length ranges of C5—C11 [109], C6—C10 [110], and C5—C6 [111]. Such liquid-like to solid-like transitions can eliminate conformational disorder, which leads to an increase in the average distance between QDs and viologen moieties in the polymer matrix, thereby decreasing the PET efficiency.

An interesting example of electron transfer depending on both the ligand length and energy level positions of the donor and acceptor has been reported [112]. In that study, assemblies of CdSe and CdTe QDs formed in an aqueous solution through electrostatic interactions of the external polar groups of surface ligands were analyzed. It was found that the interparticle distance, energy alignment of the QD band levels (i.e., the size of the QDs), and direction of the electric field between the QDs modulated the degree of CdTe QDs photoluminescence quenching. This observation was interpreted in terms of the formation of a new nonradiative relaxation pathway caused by electron transfer from the conduction band of CdTe to the conduction band of CdSe. Noteworthy, the authors have shown that simultaneous inversion of the surface charges of both CdTe and CdSe QDs (which were originally negative and positive, respectively) can block photoluminescence quenching by charge transfer. This effect can be used for differentiating between photoluminescence quenching by energy transfer and charge transfer, since the former is unlikely to be sensitive to the electric field between the particles.

Influence of the inorganic shell on electron transfer

In the case of core/shell QDs, the shell thickness has a significant effect on the rate of electron transfer. An example of this influence is presented in the study by Dworak et al. [83], where the system of CdSe/CdS QDs with a varying thickness of the shell and viologen as electron acceptor was investigated. Transient absorption spectra showed that the rate of the bleach recovery in the absence of viologen did not depend on the shell thickness. An increase in the shell thickness after addition of viologen led to a decrease in the bleach recovery rate. The authors proposed several possible explanations for this dependence: (i) the CdS shell acts as a potential barrier which drastically decreases the rate of electron transfer; (ii) the dependence of the electron transfer rate on the shell thickness reflects a decrease in the pool of MV^{2+} molecules adsorbed directly onto the CdSe core with the shell growth; and (iii) the increase in the shell thickness leads to a decrease in the effective QD band gap, which leads to a decrease in the driving force of electron transfer.

Influence of environmental and other factors on electron transfer

The environment of QDs has a significant effect on the transfer of charges and, hence, their optical properties. PET has been shown to be a solvent-dependent process [113]. The rate of PET from CdSe/ZnS QDs bearing a carboxylic acid ligand to a pyromellitimide derivative has been found to be higher in nonpolar solvents than in aprotic polar solvents. According to the diffusion-controlled electron transfer (DCET) theory [114], the probability of an electron transfer event increases with decreasing solvent polarity because of the low reorganization energy typical of nonpolar solvents.

The QD charge transfer processes in the liquid phase and in vacuum have been compared [115]. The influence of the medium on charge transfer is an important issue because QD-based systems and nanodevices are often used in an environment different from that in which they have been fabricated. For example, QDs, which are typically synthesized in colloidal solutions, are often attached to a film (in photovoltaics) or embedded into a polymer matrix. Therefore, to understand and predict the properties of QDs in their operational environment, it is necessary to fully understand all the effects that are induced by the colloidal medium used during their characterization as an individual component. Transient absorption spectroscopy in a solution and photoelectron spectroscopy in the gas phase have been used to study and compare the processes involved in charge transfer between CdSe QDs and methyl viologen [115]. Close correlation of bleaching kinetics in the gas and solution phases has led to the conclusion that neither electronic nor orientational polarization of hexane or other non-polar solvent contributes significantly to the reorganization energy term in the Marcus equation. Consequently, one should not expect solvent reorganization to considerably affect the charge migration dynamics in the CdSe—MV complex. Therefore, hexane or another non-polar solvent would provide a good environment to estimate the parameters of charge transfer in QD-based systems or nanodevice behavior in air or vacuum. On the other hand, the kinetics of charge transfer in hexane could serve as reference for the study of polar-solvent effects on charge separation and transfer in such systems.

Another type of electron transfer in QD-based systems is the transfer of the charge carrier from excited ligands to the QD conduction band. This type of electron transfer is much less studied. Bang et al. [106] investigated the

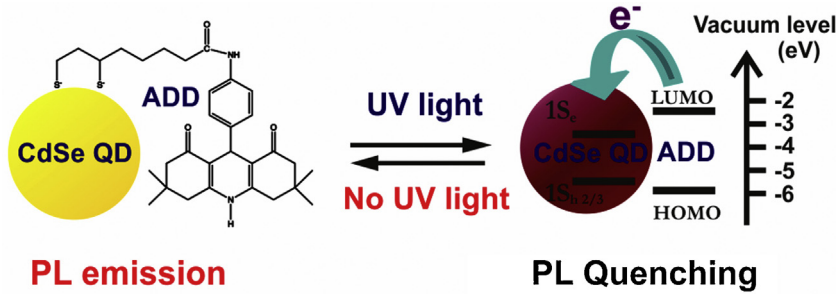

Figure 4 Schematic illustration of QD photoswitching. Potential diagrams of HOMO—LUMO levels of the acridine-1,8-dione derivative (ADD) surface molecule and 1S electron—hole levels of the CdSe QD (1.9 nm radius) are shown.
Adapted with permission from [106]. Copyrights 2012 Royal Society of Chemistry.

electron transfer from acridine-1,8-dione (ADD) to CdSe and CdSe/CdS/ZnS QDs (Fig. 4). Two excitation wavelengths, 365 and 532 nm, were used; the light with a wavelength of 532 nm excited only the fluorescence of QDs, while UV light (365 nm) excited both QDs and ADD. The excitation of ADD in this system resulted in the transfer of electron to the QD conduction band, which caused photoluminescence quenching of core CdSe QDs due to enhanced Auger recombination. In the presence of the shell, the degree of QD PL quenching was reduced, yet it was still considerable. Here, the shell played the role of a potential barrier that blocked charge carrier migration into the QD. It has been shown that the QD—ligand system studied allows the luminescence of QDs to be switched on and off by alternating excitation with visible and UV light. The ''switch on'' process, as speculated by the authors, was due to the backward transfer of injected electrons from QD's conduction band to the oxidized ADDs, which could result in overall system neutralization and facilitate reversible PL switching. Even more strong PL quenching efficiency was achieved for the complex of type-II CdTe/CdSe QDs (which have unique exciton characteristics, where the electrons and holes are spatially separated) and ADD, reaching up to 40%. Such enhancement was presumably because of the stronger overlap between the shell-localized excitonic electrons and electrons originating from oxidized ADD. The fast external light-triggered PL modulation capability can boost the application of QDs in the fields of contrast-enhanced and super-resolution imaging.

Hole transfer

Holes are another type of charge carriers formed upon photoexcitation of QDs. Like electron transfer, hole transfer can take place in QD—ligand systems. The main prerequisite for hole transfer is that the energy level of the QD valence band is lower than or equal to the ligand HOMO.

A fundamental difference of the transfer of holes from the transfer of electrons is that the bleach of QD absorption mainly depends on the population of electrons in the conduction band and is practically independent on the amount of the holes in the valence band. This observation is explained by the fact that the DOS close to VBE considerably exceeds the DOS near CBE. Therefore, the QD absorption bleach recovery rate does not strongly depend on the presence of the hole acceptor ligand [108]. Another characteristic of hole transfer is the formation of a positively charged ligand cation upon the hole transition event [108,116,117]. It has been found that, during the transfer of holes to the ligand, CdSe QD accumulates excess of excited electrons. These electrons, in turn, can react with Cd^{2+} ions to produce Cd^{+} and Cd^{0} sites in the QD structure (see Eq. (4)), but the presence of oxygen may neutralize these electrons. If the excess electrons are not neutralized with an electron acceptor or undergo charge recombination, the accumulation of electrons can further lead to cathodic corrosion and dissolution of a QD:

$$(CdSe)_n(e)_m \rightarrow (Cd^{+}Se^{2-})_m(CdSe)_{n-m} \rightarrow (Cd^{0}Se^{2-})_{m/2}(CdSe)_{n-m/2} \quad (4)$$

At the same time, the processes of electron and hole transfer have some common characteristics. It has been shown that an increase in the shell thickness of core/shell QDs leads to a decrease in the hole transfer rate [118,119]. Here, the shell acts as a potential barrier that blocks charge transfer, as in the case of electron transfer. An increase in the concentration of the hole-accepting ligand in a solution leads to a decrease in the photoluminescence intensity and lifetime [108,117—122], which is also typical of PET (Fig. 5).

Hole trapping and influence of the inorganic shell on it

Another type of charge transfer that involves holes is their trapping in trap states located inside the QD band gap. Defects of the QD structure, such as vacancies and impurities, may cause the formation of trap states into which a photo-excited electron may fall or a photo-excited hole may arise. This may result in a red shift of the QD photoluminescence or its total quenching. There are several reasons for trap state formation, including doping of QDs with various elements [123,124], nonstoichiometry of the QD surface [125], ensemble variation of the QD structure [126], presence of hole-accepting ligands [127], and chemical oxidation of QDs [128].

The authors of [126] observed the formation of additional red-shifted bands in the photoluminescence spectra of CdSe QDs with sizes from 2.3 to 7.0 nm. These bands were typically found in all photoluminescence spectra of QDs, but their contribution in larger QDs was inconspicuous compared to the band-edge photoluminescence. Comparison of the photoluminescence spectra of 2.6-nm CdSe cores and CdSe (2.6 nm)/ZnS (1.3 nm) core/shell QDs showed that the

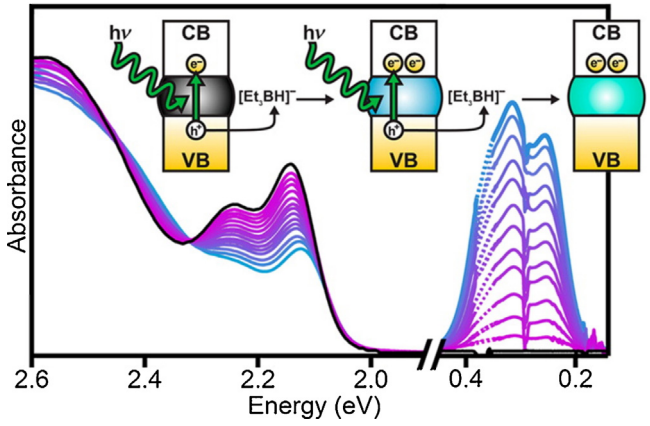

Figure 5 Top: Nanocrystal photodoping using Li[Et_3BH]. The photogenerated hole (h^+) is quenched by Li[Et_3BH], leaving an electron (e^-) in the conduction band. Further photoexcitation can add more electrons. Bottom: Absorption spectra of $d = 3.8$ nm and $d = 7.0$ nm CdSe QDs at various stages of photodoping starting from no prior photoexcitation (black) to maximum photodoping (teal). The data show exciton bleach and growth of IR absorption with photodoping. Inset: TEM images of these NCs.
Reprinted with permission from [135]. Copyrights 2015 American Chemical Society.

red-shifted band can be suppressed by coating the QD with a shell of a high-band-gap semiconductor material. This observation suggests that red-shifted luminescence is related to the trapped charge carriers localized on the QD surface. Time-resolved photoluminescence spectroscopy confirmed that holes constituted the majority of the trapped carriers in CdSe QDs. It was also shown that some of the holes became trapped for as long as tens of microseconds, and these long-lived trapped states could not decay at room temperature.

Abdellah et al. [129], studying the possibility of enhancing the performance of QD-based solar cells, investigated the influence of the thickness of the QD shell on the kinetics of hole trapping. Several batches of CdSe QDs, with different thicknesses of the ZnS shell were obtained. Mercaptopropionic acid (MPA) was used to replace the native oleate residues by ligand exchange, what caused a significant decrease in the photoluminescence quantum yield (from 14 to 0.5%) for QDs without a shell. This was attributed to the formation of numerous surface defect states acting as hole trapping centers [130] upon the sorption of MPA ligands. In contrast, CdSe QDs covered with a ZnS shell did not exhibit such a significant decrease in PL quantum yield. Thus, its value decreased from 50 to 35% after the ligand exchange for QDs protected with a 1.3-nm shell layer. It was proposed that the inorganic shell passivated the surface trap states, and an increase in the shell thickness enhanced the passivation. In order to confirm the assumption on the formation of hole trapping centers as the cause of quenching of CdSe QD photoluminescence, the authors compared the results of transient absorption spectroscopy and measurements of time-resolved photoluminescence, because transient absorption is sensitive only to the dynamics of electrons, while the photoluminescence decay kinetics depends on both electrons and holes. It was found that transient absorption kinetics did not change upon the change of the ligands, but the luminescence lifetime decreased significantly. These facts confirm that hole trapping is responsible for photoluminescence quenching, and the formation of a shell layer can inhibit this process. Furthermore, the authors showed that an increase in the shell thickness led to a steadily increased luminescence lifetime.

Influence of surface stoichiometry on hole trapping

Wei et al. [125] discuss the influence of surface nonstoichiometry on photoluminescence quenching caused by hole trapping in a system of CdS QDs with a controllable Cd-to-S ratio on the surface obtained via overgrowth of small CdS nuclei using the SILAR method [131]. It has been shown that the surface composition has a significant effect on the photoluminescence of QDs. In the case of excess sulfur atoms on the QD surface, total quenching of photoluminescence was observed; however, addition of the cadmium precursor into the QD solution led to restoration of the photoluminescence intensity. In order to understand this phenomenon, the density of states on the Cd and S sites was calculated for QDs with different surface Cd-to-S ratios using the density functional theory. In the case of Cd excess, a slight narrowing of the band gap was observed due to the appearance of energy levels at the boundaries of band gap; in the case of S excess on the particle surface, defect energy levels were formed inside the band gap. Formation of these trap levels can be explained by the fact that, in contrast to Cd ions capable of forming long Cd—Cd chains due to their metallic nature, sulfur atoms on the surface form various discrete defects, such as dangling bonds, which promote the formation of defect states. Defect states cause hole trapping and form a new way for nonradiative recombination, thereby decreasing the luminescence intensity.

The ligands themselves can form hole or electron traps and, hence, modulate the energy structure of the QD. PbSe QDs were treated with octadecylselenol in order to decrease the surface Pb-to-Se ratio [128]. A red shift of both the photoluminescence peak and the first excitonic absorption maximum was observed after the treatment of QDs with octadecylselenol. The value of the observed red shift corresponded to an increase in the QD size by 0.3 nm, which was smaller than the thickness of a single Se atom monolayer. Therefore, the authors assumed the red shift resulted from the formation of new energy levels inside the band gap, in which some of the photoexcited holes could be trapped. Comparison of room-temperature photoluminescence intensities of Se-treated and as-prepared QDs showed a decrease in the photoluminescence quantum yield of the Se-treated QDs. This may also have resulted from the appearance of Se-related trap states after the ligand treatment and formation of a separate nonradiative relaxation route that partly quenched photoluminescence by formation of a dark hole trap.

Halogenation of quantum dots for preventing hole trapping

Passivation of quantum dot surface with chlorine is an efficient strategy for removing of surface trap states, as it

was demonstrated in the work of Bae et al. [132]. Here, PbSe QDs were treated with molecular chlorine dissolved in CCl_4. It was found that chlorine oxidatively etches the surface Se atoms, forming a thin $PbCl_x$ layer, and thus removing the surface traps. The band gap of $PbCl_2$ of ~5 eV and the relative positions of its band levels when compared to PbS, PbSe and PbTe suggest a type-I alignment, where the shell confines the charge carriers inside the core of QDs, thereby enhancing radiative recombination. The latter was experimentally observed up to certain degrees of chlorine treatment, when the $PbCl_x$ layer starts to form its own new defect trap states at the core—shell interface due to the lattice mismatch between rock-salt phase of PbSe and orthorhombic phase of $PbCl_2$. Importantly, surface chlorination leading to formation submonolayer thick $PbCl_x$ shell was found to substantially decrease the susceptibility of PbSe QDs to photocharging, along with enhancement of photoluminescence, suggesting that Se trap sites affect both processes. The authors conclude that their findings in solution phase chlorination of lead chalcogenide QDs can be used in solution-processed optoelectronic applications, and are of particular interest for next-generation photovoltaics.

Unprecedented improvement of PL QY and air-stability of CdTe QDs upon their surface treatment with chloride anions was demonstrated in the work of Page et al. [133]. Near-unity quantum yields were achieved when $CdCl_2$ was used as the mildly reactive precursor of chlorine for passivation of CdTe colloidal QDs. The notable effect of such treatment was the transformation of PL decay curves into a mono-exponential ones, indicating the efficient suppression of surface trap states which rendered radiative recombination the predominant relaxation pathway. The other important finding of this work was that the suggested halide passivation strategy leads to formation of only a monolayer thin shell, yet capable of severe PL improvement comparable to a result achieved only by growing a thick inorganic shell. The increased carrier lifetime resulting from suppression of surface-trap related recombination pathways allows more time for photogenerated charges to be extracted and increases carrier mobility, both of which are likely to improve the performance of various QD-based devices.

Halide passivation not only modifies the PL properties, but also can greatly enhance carrier mobility inside a solid QD film, as it was demonstrated in the work of Ning et al. [134]. Here, PbS QDs were treated with tetrabutylammonium iodide (TBAI) in solution, and the resultant QD-based photovoltaic cells and field effect transistors made thereof have shown higher carrier mobility than the ones made of untreated QDs. Mobility is expected to be related to the density of nanoparticles in the film, thus removal of bulky oleic acid native ligands facilitated both charge carrier delocalization and hopping. A further major factor in the operation of QD-based photovoltaics and transistors is the presence of electronic trap states that are located energetically beneath the transport band. The authors hypothesize that the reduction in the density of these trap states within the bandgap achieved by surface treatment with iodine ions has led to observed order-of-magnitude improvement of electron transport when compared to the devices based on untreated QDs.

Other aspects of hole transfer

Another type of the influence of ligands on the optical properties of QDs through hole delocalization has been demonstrated [127]. Dodecylamine-coated 1.6-nm and 2.0-nm CdSe QDs were treated with phenyldithiocarbamates in order to replace the original surface ligands. This led to a drastic decrease in the observed band gap of QDs, especially pronounced in the case of the smaller nanocrystals. This effect was further enhanced upon increase in the proportion of substituent ligands compared to the original ones. It was assumed that the change in the observed band gap energy was due to the delocalization of the holes between the inorganic and organic parts of the QD caused by matching the energies of the HOMO of the phenyldithiocarbamate ligand and 1.6-nm CdSe QDs, probably accompanied by a smaller contribution of electron delocalization.

The effect of QD ''blueing'' caused by photochemical doping of the $1S_e$ levels of CdSe QDs with electrons upon anaerobic photoexcitation in the presence of $Li[Et_3BH]$, a strong hole acceptor, has been observed [135]. Filling of the QD conduction band with electrons leads to two effects visible in the absorption spectra, which can be regarded as specific signatures of the hole trapping by a strong hole acceptor: strong bleaching of steady-state absorption in the spectral region of the first excitonic transition and the appearance of a new absorption band in the IR region, which is related to intraband transitions of the electrons localized in the conduction band in the excited state. It is noteworthy that the excitonic photoluminescence is almost completely quenched after photochemical electron doping; however, upon exposure of the doped QDs to the environment, photoluminescence and other optical properties can be restored. Finally, the authors have shown that similar though less intense spectral changes arise from reduction of the QDs by biphenyl radical anions. In the case of chemical reduction, the spectral changes of QDs become less reversible, which is attributed to chemical side reactions and degradation of QDs.

Ding et al. [136] carried out a comprehensive study on the correlation between the photoluminescence quantum yield and hole trapping kinetics. They used highly emissive CdSe/CdS QDs and tunable ferrocene-based hole acceptors with various chain lengths and, hence, driving forces of hole transfer. The combination of a tunable charge acceptor and precise control over shell thickness allowed the authors to explore the hole transfer process with the rate range spanning four orders of magnitude. By studying the evolution of the photoluminescence quantum yield of core/shell QD batches with various shell thicknesses, ligand lengths, and numbers of adsorbed ligands, the authors showed that ligand-dependent photoluminescence quenching via the hole transfer mechanism could be either linearly or nonlinearly related with the ligand concentration on the QD surface, which resolves the root of contradictory data on this subject [136]. The difference in photoluminescence quenching trends is governed by the ratio between the rates of radiative decay and hole transfer (k_r and k_{HT}, respectively). In the limit case where $k_r \gg k_{HT}$, photoluminescence quenching linearly depends on the ligand concentration, whereas a strong nonlinear dependence is observed in the case of thin-shell systems and efficient hole

acceptors ($k_r < k_{HT}$), where only a few ligands per QD cause complete photoluminescence quenching.

Charge carrier transfer in QD-based systems is a process of exciton separation into electrons and holes and their segregation in different physical parts of a QD. Experimental studies show that this process can be controlled by various approaches, including modification of the inorganic structure of QDs and the structure of their surface ligands and incorporation of charge donors and acceptors into the ligand shell. The following sections of our review will focus on the use of these approaches to control charge separation and transfer in QD-based catalytic systems, photovoltaic cells, and light-emitting diodes.

Charge carrier transfer in systems of quantum dots and wide-band-gap semiconductors

Wide-band-gap semiconductors, such as TiO_2 [137,138] ZnO [139—141], and SnO_2 [142—144], are another type of electron acceptors which can drive charge carriers from QDs via charge transfer mechanisms. Systems consisting of wide-band-gap semiconductors and QDs are intensely studied because they are promising in the fields of photocatalysis [145,146], water splitting [147,148], and solar cells fabrication [141,149—152].

The driving force of charge transfer between wide-band-gap semiconductors and QDs has the same nature as that of the charge transfer from QDs to organic charge acceptors, namely, the energy difference between the band edges of the QD and the wide-band-gap semiconductor. Therefore, the general approaches that allow one to control and tune the driving force of the transfer process are the same as in the case of organic molecules. For example, the charge transfer control through modification of the QD band positions has been studied by analyzing PbS QDs with sizes of 3.8, 5.2, and 6.0 nm deposited onto the surface of TiO_2 nanobelts [153]. This system was characterized using steady-state and dynamic photoluminescence spectroscopies in order to understand the correlation between the QD size and the rate of electron transfer. Emission decay measurements showed that an increase in the QD size led to reduction of the emission decay rate for deposited QDs. In addition, it was observed that, when the amount of the QDs deposited onto the TiO_2 surface decreased, the emission decay rate rose, and these changes become less significant with increasing size of deposited QDs. Thus, deposition of any amount of 6.0-nm PbS QDs onto the surface of TiO_2 nanobelts did not lead to changes in the QD emission decay rate. The authors assumed that the differences between the photoluminescence decay kinetics of QDs of different sizes deposited on TiO_2 were due to the lowering of the PbS conduction band edge level with the growth of the nanoparticle diameter caused by the quantum confinement effect. This, in turn, led to lowering of the charge transfer driving force; for 6.0-nm QDs, the edge of the conduction band became even lower than that of TiO_2, which led to complete suppression of electron transfer and, hence, insensitivity of the QD photoluminescence decay kinetics to deposition on the surface of the electron-accepting titanium dioxide.

Similar results were obtained for CdSe QDs and TiO_2 [154]. Series of CdSe QDs with sizes between 2.4 and 7.5 nm were deposited onto TiO_2 nanoparticles, and the absorbance bleach recovery rates were compared for bare QDs and deposited ones. The rate of bleach recovery associated with the transfer of electron from the deposited QDs was higher than that of bare QDs in the solution, this rate decreasing with an increase in the size of the deposited QDs. Thus, it was confirmed that the size of the QDs, because of its close correlation with the energy positions of band edges, played the key role in the electron transfer from QDs to a wide-band-gap semiconductor.

An alternative approach to modulating the energy difference between the conduction bands of CdSe QDs and TiO_2 is to tune the band edge of TiO_2. It has been shown that protonation of the TiO_2 surface can shift the band edge of TiO_2 to more negative (relative to NHE) potentials when pH of the medium is decreased [155]. CdSe QDs were deposited onto the surface of nanostructured TiO_2 and SiO_2 films in order to investigate electron transfer in these systems [156]. Since SiO_2 is an insulator with an extremely high conduction band edge, it cannot take part in the transfer of an electron, and any kind of disparity in the kinetics of photoluminescence between TiO_2 and SiO_2 can be attributed solely to the electron transfer from QDs to TiO_2. Emission lifetime measurements showed that variation of the solution pH did not affect the emission lifetime in the CdSe—SiO_2 system, in contrast to CdSe—TiO_2, where an increase in pH was found to prolong the emission lifetimes and, hence, decrease the rate of charge transfer from QDs to TiO_2. This confirms the assumption that variation of pH of the medium can shift the position of the TiO_2 conduction band, thereby affecting the driving force of charge transfer.

Another method of boosting the charge transfer in the QD—TiO_2 system has been demonstrated in Ref. [157]. Here, CdSe QDs were bound to TiO_2 nanoparticles via a squaraine linker dye. In order to understand the mechanism of charge transfer in this system, the interaction between CdSe QDs and squaraine was investigated. It was shown that, upon linking of the dye to the QD surface, the QD luminescence intensity was considerably decreased, whereas the squaraine dye emission intensity was increased compared to the unlinked dye. It was assumed that this phenomenon resulted from energy transfer from the QD as a donor to the dye molecule as an acceptor. The overlap between the QD emission spectrum and the dye absorbance spectrum combined with direct adsorption of the dye molecule on the QD surface makes it possible for energy to be directly transferred via FRET. Furthermore, the authors used transient absorption spectroscopy to demonstrate electron transfer from squaraine to TiO_2, which was possible due to the energy difference between the LUMO of the squaraine dye (−0.91 V relative to NHE) and the conduction band edge of TiO_2 (−0.5 V relative to NHE). Since the conduction band level of CdSe QDs (−0.70 relative to NHE) lies deeper than that of the dye, the combined energy and charge transfer in the system studied allowed the researchers to increase the overall driving force of electron transfer between QDs and TiO_2, which was confirmed by an increased performance of solar cells based on the TiO_2/dye/CdSe system compared to TiO_2/CdSe (the power conversion efficiencies were 3.65 and 3.05%, respectively).

Linkers, the molecules which bind QDs with wide-band-gap semiconductors, can strongly affect the charge

transfer rate [158,159]. The influence of the type of linker molecules on the charge transfer between CdSe QDs and TiO_2 nanoparticles has been investigated [160]. CdSe QDs from three different batches were bound to TiO_2 and SiO_2 (as a neutral reference) nanoparticles via thioglycolic acid (TGA), 3-mercaptopropionic acid (MPA), oleic acid, or sulfide anion (S^{2-}). Emission decay measurements showed that the rate of electron transfer is increased in the order oleic acid < MPA < TGA < S^{2-}, the transfer being practically absent in the case of oleic acid. It was assumed that the rise of the electron transfer rate was due to the difference in the energy barrier that prevents the charge transfer, determined by the differences between the hydrocarbon chain lengths of the ligands. Thus, the shortest ligand, S^{2-}, ensured the highest rate of electron transfer in the CdSe QD/TiO_2 nanoparticle system.

Data on the influence of the nature and length of the linker molecule backbone on the electron transfer between CdSe QDs and tin dioxide nanoparticles have been published [161]. Here, *n*-methylene (HS—$[CH_2]_n$—COOH, $n = 1$, 3, 5, 7) and *n*-phenylene (HS—$[C_6H_4]_n$—COOH; $n = 1$, 2) α,ω-thiocarboxylic acids were used to bind two components with each other. Fixed sizes of both nanoparticles ensured the equality of the driving force of charge transfer in each system studied. Electron transfer was investigated using time-resolved THz photoconductivity measurements. The essence of the measurement method can be briefly described as follows. After selective absorption of a femtosecond optical pump pulse by the QD, electron transfer through the molecular bridge to the oxide nanoparticle can occur: the excess energy (ΔG) of excited electrons in the QD relative to the oxide conduction band (i.e., the driving force) triggers the electron transfer through a barrier with the potential height and width determined by the LUMO level of the molecular bridge. Free electrons populating the oxide conduction band can be selectively probed through their photoconductive response to THz pulses. The authors observed deceleration of electron transfer for both types of linkers, with an aromatic or an aliphatic backbone, with increasing bridge length; however, phenylene-based molecules exhibited higher rates of electron transfer compared to the methylene analog with the same length. DFT calculations have shown that the difference between the electron transfer rates in the systems employing these two classes of linkers is determined by two main factors. The first one is the difference in the localization of the frontier molecular orbitals: the orbitals of methylene-based linkers are compactly localized at the polar ends of the molecule, while phenylene linkers exhibit strong delocalization throughout the molecular structure. The second factor is the HOMO—LUMO energy gap, which is very large for methylene-based linkers, making the LUMO level close to the ionization threshold, and relatively low for phenylene-based linkers. Therefore, the height of the potential barrier for electron transfer is considerably lower for the latter linkers, which means that the aromatic *n*-phenylene bridges allow faster electron transfer from CdSe QDs to SnO_2 nanoparticles compared to *n*-methylene ones. Finally, the authors note that their data quantitatively agree with the data on the conductance through single molecules and self-assembled monolayers, which indicates that the conductance and electron transfer rates are indeed closely correlated. This has allowed the authors to assume analogy between simple resistors to current flow and the molecular bridges sandwiched between the QD donor and the oxide acceptor, where higher concentrations of electrons in the phenylene moieties compared to methylene ones correspond to the differences in resistance.

Similar results have been obtained in a study on the influence of the nature of the linker molecules on the electron transfer from CdSe QDs to ZnO nanowires [162]. The authors showed that a simple rectangular barrier tunneling model was insufficient for explaining the difference between electron transfer rates in three systems in which QDs and ZnO nanowires were bound via structurally similar linkers: mercaptoacetic acid (MAA), 2-mercaptopropionic acid (2MPA), and 3-mercaptopropionic acid (3MPA). Specifically, it was found that the rates of electron transfer through MAA and 2MPA molecules, which had almost equal lengths and LUMO energies, differed by a factor of more than three. Then, the authors used the bridge-mediated electron-transfer theory [163] to show that electron transport rate strongly depended not only on the LUMO energy of the linker molecule, but also on the topology of the frontier orbital of the molecular linker, especially the orbital amplitudes at the terminal atoms, where the electron enters and leaves the molecule. Apart from the type of the linker, its concentration in the solution during exchange of the QD original ligands and the method of QD deposition onto the semiconductor have been shown to be important factors of the electron transport kinetics [164]. In that study, β-alanine (β-Ala) was used as a binder between CdSe QDs and a TiO_2 mesoscopic film in order to estimate the applicability of trap-state-remediating amine compounds as linkers at the QD—metal oxide interface of QD-sensitized solar cells. An advantage of β-alanine is its Lewis basicity, owing to which its binding to the QD surface leads to passivation of the QD surface trap states, in contrast with the generally used thiol-based linkers, such as short mercaptoacids. Indeed, a considerable increase in the CdSe QD photoluminescence quantum yield was observed upon addition of β-Ala to the QD solution to a concentration of approximately 0.08 mM (~17 β-Ala ligands per QD). However, at higher concentrations of the ligand, the photoluminescence quantum yield drastically dropped, which was explained by the fact that, in addition to the trap-state passivation, β-Ala plays an important role in reducing the electron—hole wave function overlap in the QD [165]. Femtosecond transient absorption spectroscopy was used to correlate the charge transfer rate in the CdSe QD—TiO_2 system and the concentration of β-Ala in the ligand exchange solution [164]. Fig. 6 shows the results of this study, along with the evolution of the photoluminescence quantum yield described above. The authors presumed that the decline of the electron transfer rate constant (k_{et}) in the low concentration window (region I) was likely to be caused by charging of the QD surface, which led to enhanced confinement of the photogenerated electron in the QD core by the β-Ala linkers through Coulombic repulsion. The subsequent increase in k_{et} in region II (Fig. 6) was apparently caused by intense hole trapping. Although hole trapping occurred in region I, the probability of hole trapping (k_{ht}) was minimal here due to the presence of only a small amount of β-Ala on the QD surface. In the high linker concentration window, hole trapping

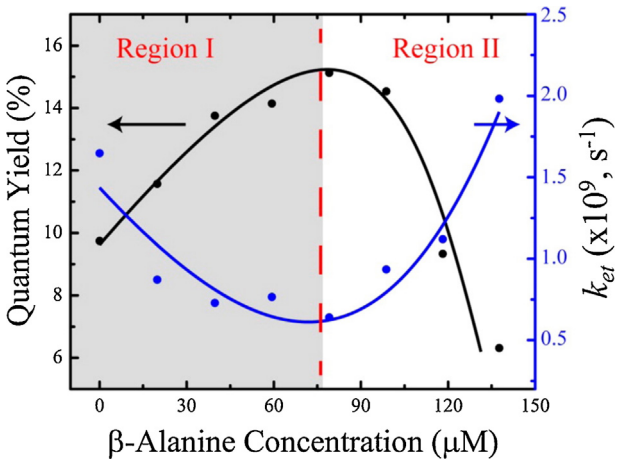

Figure 6 Fluorescence quantum yield (black) of β-Ala-modified QDs suspended in toluene plotted in comparison with k_{et} (blue) of these samples deposited onto TiO_2.
Reprinted with permission from [164]. Copyrights 2013 American Chemical Society.

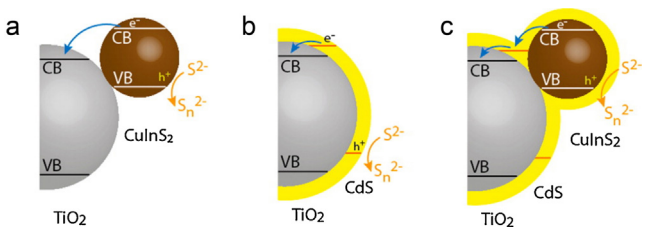

Figure 7 Schematic microstructure and the band energy diagram for (a) $TiO_2/CuInS_2$, (b) TiO_2/CdS, and (c) TiO_2/composite showing the different possibilities of electron transfer from QDs to TiO_2.
Reprinted with permission from [166]. Copyrights American Chemical Society.

became more prominent and activated charge separation in QDs, thus increasing the rate of electron transfer. It was also shown that the method of QD deposition onto TiO_2 nanoparticles had a significant effect on the rate of electron transfer [164]. Comparison of the two deposition methods that employ β-Ala linkers, one of which resulted in partial passivation of the QD surface (here, TiO_2 nanoparticles were treated with linker molecules prior to deposition of TOPO-coated QDs), and the other one ensured complete encapsulation of QDs through preliminarily coating them with linkers, showed a threefold higher rate of electron transfer in the former case. However, in both cases, the electron transfer rates were sufficiently smaller than those in the system where TOPO-coated QDs were directly deposited onto TiO_2 nanoparticles.

The high efficiency of electron transfer from QDs directly deposited onto wide-band-gap semiconductors can be further improved by forming a semiconductor overlayer [166]. $CuInS_2$ QDs were directly deposited onto TiO_2 nanoparticles without the use of linker molecules. Efficient electron transfer in this system was confirmed by the difference in the absorption bleach recovery kinetics between the $CuInS_2$—TiO_2 and $CuInS_2$—SiO_2 systems. The rate of the bleach recovery was significantly higher in the former system, which confirmed electron transfer from QDs to TiO_2 as an excitation relaxation pathway. Deposition of a CdS layer on top of $CuInS_2$ QDs electrophoretically deposited onto a TiO_2 mesoscopic film using the SILAR technique was shown to cause a twofold improvement of the QD-sensitized solar cell performance. This effect was accounted for by the formation of a direct $CuInS_2 \rightarrow CdS \rightarrow TiO_2$ cascade electron flow caused by favorable energetics of the three-component system. As shown in Fig. 7c, the levels of the conduction bands of bulk CdS, $CuInS_2$, and TiO_2 (−1.0, −0.95, and −0.5 V relative to NHE, respectively) favor cascade electron hopping in such a ''common shell'' system. This mechanism of mediated electron transfer is believed to provide better charge separation, transfer, and overall photovoltaic performance than those in the $TiO_2/CuInS_2$ and TiO_2/CdS systems [166].

Formation of a shell atop the QD core resulting in a type I heterostructure, while being expected to hinder charge transfer by creation of a potential barrier for the excited carriers [55,167], still can improve the charge transfer from QDs to a wide-band-gap semiconductor by passivating the nonradiative trap states on the QD surface [168]. In Ref. [163], electron transfer from $CuInS_2/CdS$ and $CuInS_2/ZnS$ core/shell QDs to a sintered TiO_2 nanoparticle film has been investigated, the difference between the QD photoluminescence lifetimes upon their deposition onto TiO_2 and SiO_2 (the latter served as a non-acceptor reference) being used to estimate the charge transfer rates and efficiencies. The electron transfer rates and efficiencies of ZnS- and CdS-coated $CuInS_2$ QDs were found to decrease with increasing shell thickness; the value of this decrease, which was in all cases higher for ZnS-coated QDs, was shown to be correlated with the height of the potential barrier created by the shell material, and, hence, the degree of electron delocalization into the shell. However, the results of experiments with 2.0-nm $CuInS_2$ cores coated with a CdS shell showed a deviation from this dependence. While electron transfer efficiency was found to continuously decrease with increasing the thickness of the shells over large (3.6-nm) cores, the growth of CdS shells over the smaller (2.0-nm) cores led to an initial rise of the electron transfer efficiency form 66 to 82%. This difference was attributed to passivation of surface defects acting as nonradiative recombination centers competing with electron transfer. Thus, for smaller cores, passivation of surface defects outweighed the creation of a potential barrier when the shell was sufficiently thin, while the low potential barrier created by CdS allowed the electron transfer to remain highly efficient. This was observed until the shell thickness was reached at which the effect of the potential barrier became much stronger than the effect of trap passivation.

The difference between electron transfer from the band-edge and trap states of CdSe to metal oxide semiconductor nanoparticles has been analyzed [169]. Two types of CdSe QDs were obtained, the first exhibiting only band-edge emission (QD A), and the second one exhibiting both band-edge and trap-state emissions (QD B). In order to investigate the electron transfer, QD A and QD B were bound to TiO_2 or ZrO_2 nanoparticles using mercaptopropionic acid as a linker molecule. Luminescence quenching measurements have shown that the electron injection into TiO_2 can occur both from the conduction band-edge and trap states of CdSe

QDs, as evidenced by an increased dynamic quenching of both band-edge and trap-state emissions. Estimation of the dependences of the band-edge and trap-state photoluminescence quenching on the excitation wavelength has shown that only the trap-state charge transfer efficiency was sensitive to the excitation wavelength, being decreased as electrons became trapped more deeply. The most probable explanation of this effect is a decline of the driving force of electron injection. Hence, the results obtained in Ref. [169] clearly demonstrate that trapped electrons play significant and often negative role in the charge transfer in QD-based systems.

The possibility of tuning the effectiveness and direction of charge transfer in complex 0D—1D nanostructures by finely selecting the energy levels of the components has been demonstrated by Han et al. [170]. The authors immobilized ~4-nm CdSe QDs onto high-aspect-ratio Tb-doped $CePO_4$ nanowires by means of hydrogen bonding between the surface ligands of QDs (either TOPO/HDA mixture or 2-aminoethanethiol) and water molecules within the nanowires and on their surface. The resulting nanoscale CdSe QD—$CePO_4$:Tb heterostructures displayed photoluminescence quenching and shorter lifetimes compared to unbound CdSe QDs and $CePO_4$:Tb nanowires. The assumption on quenching via energy transfer was rejected, because the spectral overlap between the possible donors and acceptors in the system was negligible. Therefore, the photoluminescence quenching was primary attributed to photoinduced charge transfer in the 0D—1D nanoheterostructure upon excitation. It is noteworthy that the system studied had different spectral signatures and quenching dynamics in the cases of excitation at 375 and 280 nm. Considering that the valence band of QDs in the complex was at a slightly lower level than the valence band of $CePO_4$:Tb nanowires, and the conduction band of the latter was considerably higher than that of the former, the authors have concluded that there are two possible mechanisms of QD photoluminescence quenching involving charge transfer. Specifically, upon excitation in the near-UV to visible region (375 nm and above), hole transfer from CdSe QDs is prevailing, while in the case of deep-UV excitation (280 nm and below), electron transfer predominantly occurs from $CePO_4$:Tb to CdSe QDs. These results are considered to have implications for designing novel photovoltaic architectures capable of harvesting UV light, as well as promoting highly efficient charge separation [170].

After this summary of the major pathways of charge transfer in QD-based systems and methods for controlling them through modification of either the inorganic part of the QDs or their organic shell, we will now turn to applications of QDs in the areas where charge transfer is used for engineering of photocatalysts, light emitting diodes (LEDs) and photovoltaics (PVs).

The use of charge transfer in quantum dot-based systems and devices

Quantum dot-based photocatalysis

The use of photocatalysis utilizing free solar energy to obtain a useful effect is an important task in many fields of modern life and technology, from hydrogen production and tough chemistry to environment protection and public health. Typical applications of photocatalysis are, e.g., water splitting [171,172], oil chemistry [173], processing of toxic residues and decontamination of waste waters [174—176], and non-fouling coatings [177,178]. The most common photocatalyst for modern technology is TiO_2 [179]. Its wide use is due to its low cost, low toxicity, and well-developed techniques of production. However, TiO_2 has a significant disadvantage as a photocatalyst because of its relatively low photoactivity under visible light irradiation resulting from its wide band gap. QDs are a new promising material for photocatalysis which can be active under irradiation with visible light. QDs can sensitize commonly used photocatalysts, such TiO_2 [180] and ZnO [181,182], or act themselves as photocatalysts [183] for both oxidation [184,185] and reduction [146,186] because of their narrow and tunable band gaps and capacity for effective charge separation. Since oxidation and reduction reactions involve transfer of electrons, all the approaches to controlling and improving it described in the previous sections are relevant to photocatalysis.

Surface ligands are an important aspect in QD-based photocatalysts, because the substrate molecule should be as close to the QD surface as possible for charge transfer, the elementary act of photocatalysis, to proceed. The easiest way to ensure intimate contact of the phototreated substance with the QD is to strip off the ligand shell [187]. In Ref. [187], the photocatalytic activity of CdS QDs was considerably enhanced compared to the commonly used MPA-capped QDs by means of the ligand-stripping procedure. After the synthesis, organic-soluble CdS nanocrystals were treated with trimethyloxonium tetrafluoroborate and DMF to obtain aggregated but very active photocatalyst particles at neutral pH. The activity of these QDs in the hydrogen evolution reaction was further enhanced by addition of bivalent cobalt as a co-catalyst. Note that the origin of cobalt had no effect on the final activity of the QDs in photocatalysis: systems employing a simple cobalt salt or the efficient sensitizing dye cobaloxime exhibited about the same activity after a short incubation period. The authors have concluded from these data that cobalt precursors decompose during the incubation period, and the product decomposition accumulates at the surface, forming active catalytic species. In contrast to ligand-stripped QDs, MPA-capped QDs exhibited only a weak activity in evolution of hydrogen after treatment with a co-catalyst, which allowed the authors to assume that MPA interfered with the activity of the QD-MPA/Co system primarily because it acts as a physical barrier; another possible cause was the prevention of nanoparticles from forming branched QD aggregates, thereby precluding efficient charge separation and transport in the branched QD aggregate.

Alternatively, the removal of ligands has been shown to facilitate selectivity enhancement of the photocatalytic decomposition of formic acid [188]. In Ref. [187], the same system of CdS QDs and cobalt co-catalyst was shown to selectively catalyze decomposition of formic acid into H_2 and CO_2 when the pure substrate was used as a medium. It should be noted that MPA capping was necessary to ensure an unprecedented efficiency of the catalyst with a turnover number greater than 6×10^5. The transfer of the catalysis

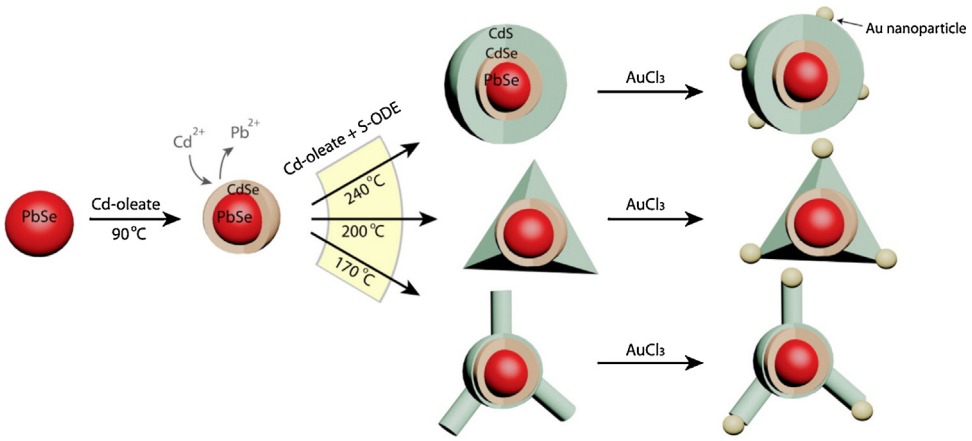

Figure 8 Schematic description of the synthesis of PbSe/CdSe/CdS NHSs and Au-tipped PbSe/CdSe/CdS NHSs with varying morphologies.
Reprinted with permission from [190]. Copyrights 2012 American Chemical Society.

system into the aqueous media decreased its efficiency; the reaction pathway was also altered, with formic acid decomposed into CO and H_2O. The authors found that selectivity switchover to CO was determined by the basic aqueous environment. After the transfer to an aqueous solution, the initially deteriorated photocatalytic activity of QDs was restored and even considerably enhanced (with a turnover number of 3×10^6) when the ligands were stripped off using trimethyloxonium tetrafluoroborate and DMF.

If the substrate molecules have appropriate polar groups that can attach to the surface of QDs, they can themselves become surface ligands, thus removing the obstacle for charge transfer. Photocatalyzed formation of carbon disulfide via photoinduced hole transfer from QDs to 1,1-dithiooxalate (DTO) has been demonstrated [189]. The CdSe-DTO system was obtained by exchanging the original myristate ligands to DTO, which caused significant photoluminescence quenching. This was attributed to hole transfer from QDs to DTO. The authors assumed the following mechanism of DTO cleavage:

$$S_2CO_2^{2-} \rightarrow CS_2 + CO_2 \quad (5)$$

In order to test this hypothesis, the QD—DTO system was irradiated at a wavelength of 365 nm, which was slightly above the absorption band of DTO. This irradiation resulted in a systematic decrease in the absorption rate at 335 nm (the wavelength of DTO absorption), which indicated photodecomposition of the surface-coordinated DTO molecules. At a higher rate of photochemical conversion the QDs precipitated because of the loss of the water-solvating surface ligands. Aeration of the reaction mixture was found to strongly promote photodecomposition of DTO, which was explained by the formation of DTO radical anion as a reaction intermediate; oxygen as the ultimate electron acceptor quenched the radical, pushing the reaction toward the final decomposition product. Apparently, the findings show a potential pathway for systematic removal or complete replacement of QD surface ligands, which is necessary for controlled photochemical syntheses of new QD—ligand conjugates [189].

The QD photocatalytic performance can be considerably improved through heterostructuring, with QDs bound to another semiconductor or wide-band-gap oxide, which maximizes the charge separation and decreases the probability of charge recombination [190]. In Ref. [190], the photocatalytic activity of Au-tipped PbSe/CdSe/CdS core/shell/shell nanoheterostructures (NHSs) with type II or quasi-type II band offsets was estimated in the reaction of the methylene blue reduction under infrared irradiation. By varying the synthesis temperature at the last stage, nanostructures with three different morphologies were obtained: spheres, pyramids, and tetrapods (Fig. 8). Gold nanoparticles were grown at the most reactive sites of the obtained nanostructures, namely, tips or corners. These Au nanoparticles play the role of electron scavengers: electron localization in the Au nanoparticles increases the photocatalytic efficiency of the whole NHS by reducing the electron—hole overlap. The heterostructuring approach allowed the formation of staggered band potential offsets for the electrons, thereby ensuring photocatalysis, which was impossible in the case of single-component nanocrystals. The differences in performance between the three morphologies studied were determined by their differences in the effective hole tunneling distance, i.e., the distance that a hole should travel to localize at the surface and to contact with the substrate molecule. In the case of the spherical NHSs, which displayed the least photocatalytic activity, electron—hole pairs remained separated for a longer time compared to the other nanostructures, and holes confined in the PbSe core could not reach the nanocrystal surface for the oxidation of methanol, a sacrificial hole scavenger. Conversely, in the tetrapod NHSs, the width of the CdS shell (hole barrier) at the body of the tetrapod, was significantly smaller compared to the other morphologies, as was shown by TEM. Combined with the extended CdS arms tipped with Au nanoparticles, which drive charge separation, the tetrapod-shaped NHSs exhibited a substantially higher photocatalytic efficiency than the pyramidal NHSs, let alone nanospheres. Thus, it has been concluded [190] that charge separation cannot entirely account for efficient photocatalysis, and accessibility of the substrate molecule for a hole in the ''open'' structures, such as pyramids and tetrapods, is the key factor to be considered in designing of photocatalysts.

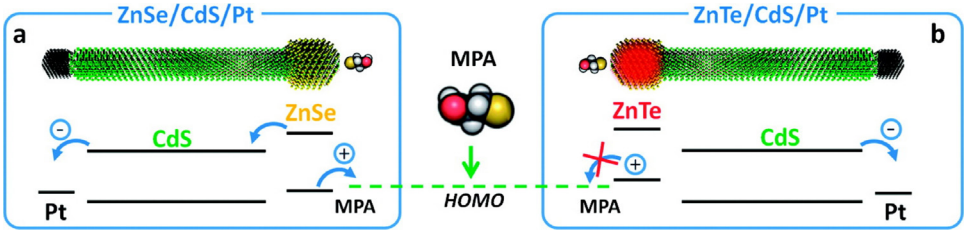

Figure 9 Electronic level diagram showing a relative alignment of excited state energies in ZnSe/CdS/Pt (a) and ZnTe/CdS/Pt (b) heteronanocrystals.
Reprinted with permission from [191]. Copyrights 2012 American Chemical Society.

Another example of the nanoheterostructuring approach is presented in Ref. [191]. Two types of heterostructured Pt-tipped dot-in-a-rod nanoparticles (ZnSe/CdS/Pt and ZnTe/CdS/Pt) capped with mercaptopropionic acid (MPA) were tested as photocatalysts for water splitting. The components of the composite were selected in such a way that a linear energy gradient was formed that could drive photoinduced charge carriers to localize in the opposite parts of the nanorod (Fig. 9). It was experimentally found that ZnSe/CdS/Pt heteronanorods, but not ZnTe/CdS/Pt ones, exhibited a high photocatalytic activity. This phenomenon can be explained as follows: the valence band edge of ZnSe is lower than the HOMO of MPA; therefore, this heterostructure can efficiently expel photoinduced holes to the surface via ZnSe-to-ligand charge transfer, thereby ensuring reaction flow and preventing the degradation of the semiconductor metal composites. When ZnTe is used as the tip, the hole transport to the MPA ligand is hindered, because the band edge of ZnTe is at a higher energy level than the HOMO of MPA. The absence of hole transfer leads to their increased concentration in the ZnTe tip, resulting in a higher probability of charge recombination and degradation of the nanorod as a consequence of photoinduced oxidation. Furthermore, it was found that, when dissolved MPA was completely oxidized, photocatalysis stopped even if ZnSe/CdS/Pt heterostructures were used. Addition of MPA to the solution led to restoration of the photocatalytic properties of nanoheterorods, and hydrogen evolution occurred at the same rate. These findings highlight the importance of selecting suitable energy parameters of the components of a ligand—semiconductor system for improving both the efficiency and the stability of homogeneous photocatalytic water reduction in the presence of sacrificial agents.

As noted above, surface trap states slow down the transfer of electrons outside of QDs. The same problem arises in the case of QD-based photocatalysis. The photocatalytic H_2O splitting activities of CdSe and CdSe/CdS core/shell QDs were compared to clarify the effect of the CdS shell on the efficiency of this process [192]. The photocatalytic activity of CdSe/CdS QDs in the reaction of water splitting was found to be ten times higher than that of CdSe QDs. This enhancement was attributed to the passivation of deep surface trap states found in bare CdSe cores, which maintained the reduction potential determined by photogenerated electrons at a sufficient level for reduction of water. Although, in the core—shell system, photogenerated electrons have to tunnel through the shell for the catalytic reaction to occur, this barrier only weakly affects the efficiency of photocatalysis, because the electron tunneling rate is three orders of magnitude higher than the minimum rate required for catalysis.

Another common approach in QD-based photocatalysis is decoration or sensitization of wide-band-gap semiconductor nano- or microstructures with QDs. This approach benefits from both the high absorbance of QDs in the visible or near-infrared spectrum and high efficiency of charge carrier scavenging by wide-band-gap semiconductors [193]. TiO_2 nanotubes (TNTs) were decorated with CuS QDs by sequential treatment of TNTs with cysteine, copper (II) acetate, and Na_2S. As a result, 3- to 4-nm CuS QDs were formed on the surface of the oxide nanotubes. It was shown that decoration of TiO_2 improved the photoresponse in the visible and near-infrared regions, and the photoactivity of CuS/TNTs remained high even when they were irradiated at wavelengths longer than the exciton absorption wavelength of the TiO_2 nanotubes. These results suggest that CuS QDs can be used as a co-catalyst to widen the usable absorption band of TNTs.

It is noteworthy that silicon QDs, which are barely stable under ambient conditions because of oxidation by atmospheric oxygen, could still act as photocatalysts. Hydrogen-terminated Si QDs (H-Si QDs) prepared by the electrochemical etching method were shown to be excellent photocatalysts for CO_2 reduction and dye (methyl red) degradation [194]. The photocatalytic activity of silicon QDs was found to be size-dependent: 1- to 2-nm Si QDs effectively catalyzed the reduction of carbon dioxide to formaldehyde and formic acid, while their larger counterparts had almost no catalytic activity. The authors assumed that this was because only in the smaller Si QDs did the excited electrons have sufficient energy to induce photochemical reduction of CO_2/CO_3^{2-} or degradation of the dye upon irradiation. Note that larger (3- to 4-nm) Si QDs catalyzed the oxidation of aromatic compounds to aryl alcohols in the presence of hydrogen peroxide. Formation of a thin SiO_2 shell atop the silicon QDs was found to be critical in this process, with SiO_2 serving as the actual catalyst of the hydroxylation of aromatic compounds. The authors conclude that cadmium-free silicon QDs could serve as a versatile photocatalyst for reduction, decomposition, and selective oxidation and be used as building blocks of novel complex nanostructured catalysts.

Light-emitting diodes

Light emitting diodes (LEDs) are of major importance in the modern world. LEDs are basic components of displays

in almost every stationary or portable electronic device. Semiconductor QDs, with their unique optical properties, including color tenability, high color purity, near-unity photoluminescence quantum yield, and high color reliability, offer great prospects in development of a new generation of LEDs and displays. Basically, there are two types of QD-based LEDs (QD-LEDs): those operating on the principle of down-conversion, where QDs are used as phosphors to saturate the emission of blue LEDs to white light spectrum, and electroluminescent (EL) LEDs. The principle of EL QD-LED operation is carrier transport through charge-transport layers and direct injection of the two types of carriers into QDs, where they can recombine with emission of a photon. Here, we will focus on EL QD-LEDs, because their operation is closely related to the properties of charge transfer in QDs, and the performance of these devices can be tuned to some extent by control over charge transfer.

Like widely used organic light emitting diodes (OLEDs), EL QD-LEDs are commonly designed as multilayer structures, in which QDs are incorporated as an active layer sandwiched between charge-transport layers. The efficiency of a QD-LED is mainly determined by the balance between the rates of charge carrier transport from the electrodes to the active layer and the rate of their transfer into QDs, where the carriers finally recombine. Therefore, the major part of the studies dealing with QD-LEDs are aimed at selecting optimal electron and hole transport layer materials [195—200]. In general, the results of these studies show several important conditions that should be met for efficient QD-LED operation. First, the HOMO energy levels of the hole transport layer (HTL) material should facilitate the injection of holes into the VBE of QDs; at the same time, the HTL should have energy barriers for electrons to prevent them reaching the anode. Similarly, the electron transport layer (ETL) should act as a barrier for holes heading toward the cathode, and both HTL and ETL should have sufficient energy gaps between the HOMO and LUMO in order to minimize the absorption in the visible spectral region. Fine matching of the energetics at the interface between the transport layers and the QD emissive layer may be achieved by introducing a thin interlayer [201]. In Ref. [200], a layer of 1,3,5-tris(N-phenylbenzimidazole-2-yl)benzene (TPBi) as thin as 7 nm was introduced between the QD emission layer and the 4,4-N,N-dicarbazole-biphenyl (CBP) HTL in order to control the energy-level alignment at the HTL—emission-layer interface. The benefit of the introduction of this interlayer was that the charge accumulation zone and the exciton formation zone became spatially separated as a result of a larger energy mismatch between the HOMOs of CBP and TPBi than between the HOMO of TPBi and the QDs valence band, which prevented the associated exciton quenching and improved the performance of the QD-LED device. Specifically, a 3.5-nm TPBi interlayer determined a 46% enhancement of the peak efficiency.

The surface ligands of QDs considerably influence the parameters of charge transfer outside and inside of the QDs. Since the efficiency of QD-LEDs is closely correlated with the relative charge transport and transfer rates, modification of surface ligands is a potential approach to controlling the device operation. The efficiency of QD-LEDs with long- and medium-chain aliphatic ligands on the surface of CdSe/ZnS QDs is twice higher than that of QD-LEDs where aromatic ligands are used [202]. The difference in the performance is assumed to result from stronger exciton localization in the case of aliphatic ligands, which is supported by a weaker conductance of the ligands themselves and a more sparsely packed QD layer.

The influence of the QD surface ligands on the performance of QD-LEDs has been investigated in more detail in Ref. [203]. Here, octadecylamine coating Mn-doped ZnS QDs after the synthesis was exchanged to a series of alkyldithiols with various chain lengths, including 1,2-ethanedithiol (EDT), 1,4-butanedithiol (BDT), 1,6-hexanedithiol (HDT), and 1,8-octanedithiol (ODT). Manganese doping prevented photoluminescence quenching due to trap formation caused by thiol ligands, which normally boost nonradiative recombination. The dependence of the QD-LED performance on the type of the dithiol ligands was complex. It was found that the electroluminescence intensity and external quantum efficiency of EL QD-LEDs made of QDs with different ligands decreased in the following order: HDT > ODT > BDT > EDT; i.e., for the performance of the QD-LEDs to be maximum, the ligands had to be neither too short nor too long. This has been explained by variation of the QD film conductance depending on the density of QD packing, which, in turn, depended on the ligand length. Thus, the authors conclude that there is an optimum length of the QD ligands ensuring the highest performance of the device. For this particular system, 1,6-hexanedithiol has been found to be the optimal ligand [203].

An intriguing approach to encapsulation of CdSe/ZnS QDs using poly(*para*-methyl triphenylamine-*b*-cysteamine acrylamide) block-co-polymer (PTPA-*b*-CAA) and its application to EL QD-LED was demonstrated in Ref. [204]. Two types of QD-LED were fabricated, based on either oleic acid-capped QDs or block copolymer-capped ones. In the case of block copolymer capping, a threefold increase in the external quantum efficiency of the device was observed. This increase of performance was attributed to the specific properties of the PTPA-*b*-CAA coating of QDs, which facilitated injection of holes into the QDs by matching of the HOMO level of the PEDOT:PSS hole-transport layer and the valence band of QDs. Moreover, the PTPA-*b*-CAA coating allowed the formation of a very uniform QD layer, filling the voids between adjacent QDs. This uniform and solid film ensured suppression of the possible current leakage from the direct contact between HTL and ETL through interstitial voids or defects in the case when the active emission layer consisted of oleic acid-capped QDs.

Photovoltaics

At present, solar cells account for a significant part of the world's green energy production. In the past decades, considerable progress has been made in the field of organic and dye-sensitized solar cells in terms of power conversion efficiency. Their specific advantages of flexibility, transparency, and the possibility of large-scale production using solution-based processes make them promising candidates for the replacement of the widespread silicon solar cells, which are costly but still more efficient thus far. QDs, being very effective in absorption of light in a wide spectral range and transformation of the absorbed energy into the energy of

excited charge carriers, have found their niches in every type of prospective solar cell designs [205].

Robel et al. [206] carried out one of the pioneering studies on QD-sensitized solar cells (QDSCs). Having successfully immobilized ~3-nm CdSe QDs onto dispersed TiO_2 nanoparticles with the use of HOOC-R-SH bifunctional linker molecules (R = C1, C2, or C15), the authors have observed quenching of QD photoluminescence and alteration of bleaching kinetics in transient absorption spectra. These findings clearly demonstrated fast charge separation and transfer in the composite CdSe—TiO_2 system (within picoseconds), which encouraged the authors to design a three-electrode photoelectrochemical cell using a transparent electrode covered with a mesoscopic TiO_2 film as a base for sensitization. QDs were immobilized on the electrode by a method similar to that used previously for the colloid system with the use of the same type of linkers. Measurements of the incident photon to current conversion efficiency (IPCE) have shown that the electrodes fabricated using mercaptohexadecanoic acid (MDA) and mercaptopropionic acid (MPA) as linkers have almost the same maximum efficiencies and similar spectral responses, while those where thiolacetic acid (TAA) served as a linker was less efficient (maximum IPCE of 9% of the). In contrast to organic-die-sensitized solar cells, which exhibit steady photocurrent immediately after excitation, in QD-sensitized ones, both photocurrent and photovoltage rapidly rose and then drastically decreased within the first 30 s of illumination, before stabilizing. The assumption that this current instability resulted from inability of the redox couple to quickly scavenge photogenerated holes was rejected by the authors, because the initial current decay became even more predominant at higher concentrations of Na_2S, which was used as an electrolyte in the cell, although an increased electrolyte concentration was expected to enhance hole scavenging. An alternative explanation of the rapid photocurrent decay was increased concentration of charge carriers at the CdSe—TiO_2 heterointerface and contribution of internal grain boundaries, which led to recombination losses and charge scattering. Experiments with various excitation powers showed that the latter hypothesis was true, because an enhanced excitation power led to a greater decay of photocurrent, while at a low excitation power, the operation of the photoelectrochemical cell was stable. Because the injection of electrons into TiO_2 is an ultrafast process (femtosecond—picosecond time scale) and transport of electrons across the nanostructured film is relatively slow (on the microsecond to millisecond scale), electrons begin to accumulate within the mesoporous TiO_2 network, and the charge harvesting efficiency of the cell decreases with increasing excitation intensity. Therefore, the authors conclude that suppressed electron transport in the TiO_2—CdSe composite restricts optimal performance of the cell at higher light intensities and shows that the charge transport across the TiO_2 film is the main limiting factor in CdSe QD-based solar cells [206].

The performance of PbS-based solar cell has been significantly improved through surface modification of PbS QDs [207]. As-synthesized QDs were treated with tetrabutylammonium iodide (TBAI) and 1,2-ethanedithiol (EDT) organic ligands in a solid-state ligand exchange procedure. The cells fabricated using only TBAI-treated PbS QDs had a power conversion efficiency of 6%, while replacement of the topmost QD layers with PbS—EDT resulted in a ~35% increase in the power conversion efficiency (to 8.2%). This improvement was attributed to the band offsets formed between the two PbS QD layers with different cappings, which effectively blocked electron flow to the anode while facilitating hole extraction.

The effect of surface trap states in QDs on the function of QDSCs has been demonstrated by Ehrler et al. [208] The performance characteristics of PbSe and PbS-based depleted heterojunction solar cells were compared, and it was found that the power conversion efficiency of PbSe-based devices approached 3%, which was threefold higher than that of PbS-based ones. This difference was explained by a higher density of intragap states in PbS QDs than in PbSe QDs, which was confirmed by XPS, UPS, IR absorption, and transport measurements; this enhanced charge carrier recombination at the PbS—ZnO heterointerface. However, the authors have found a way to limit this carrier recombination by reducing the concentration of carriers in the ZnO electrode by doping the electrode with nitrogen atoms. The open-circuit voltage and efficiency of PbS QD—ZnO devices were increased by 50% upon doping of ZnO with nitrogen, which shows that this method is efficient for control over interface charge carrier recombination in systems prone to this phenomenon.

As in the case of charge transfer in QD—ligand system, charge transfer in QDSCs has a parameter that can be compared to driving force, since it determines the rates of separation of the charge carriers and collection of them at the electrodes. In the case of QDSCs, this parameter is the difference in the energy between the HOMO level of the donor and the LUMO level of the acceptor [209,210]. It has been demonstrated [211] that this parameter can be increased by introducing molecules of an ionic liquid, e.g., 1-benzyl-3-methylimidazolium chloride, between the layers of PbS QDs and phenyl-C61-butyric acid methyl ester (PCBM) (Fig. 10). Incorporation of the ionic liquid layer into the device improved the compatibility between the donor and acceptor layers, which was confirmed by a decrease in charge transfer resistance. Formation of the spontaneous dipole layer shifted the band edge of PCBM closer to the PbS vacuum level, which enhanced the device performance, whose power conversion efficiency was increased from 1.62% to 2.21%.

Colloidal quantum dots have proved to be promising for modern technology. The ease of controlling charge transfer processes and, hence, the overall operation of a nanodevice by variation of QD structure or surface parameters allows their ubiquitous use to be expected in the near future. However, we should always be aware of nanotoxicity issues [212,213] and take them into account in engineering of nanostructure-based systems in order to make use of the great potential of these unique nanomaterials without compromising environmental safety and human health.

Summary and outlook

Historically, applied research in QDs has been focused on optimization of their inorganic part by improving the crystallinity of QD cores, coating them with epitaxial shells, and seeking for novel QD designs (e.g., multishell structures) that could improve the luminescence or other properties

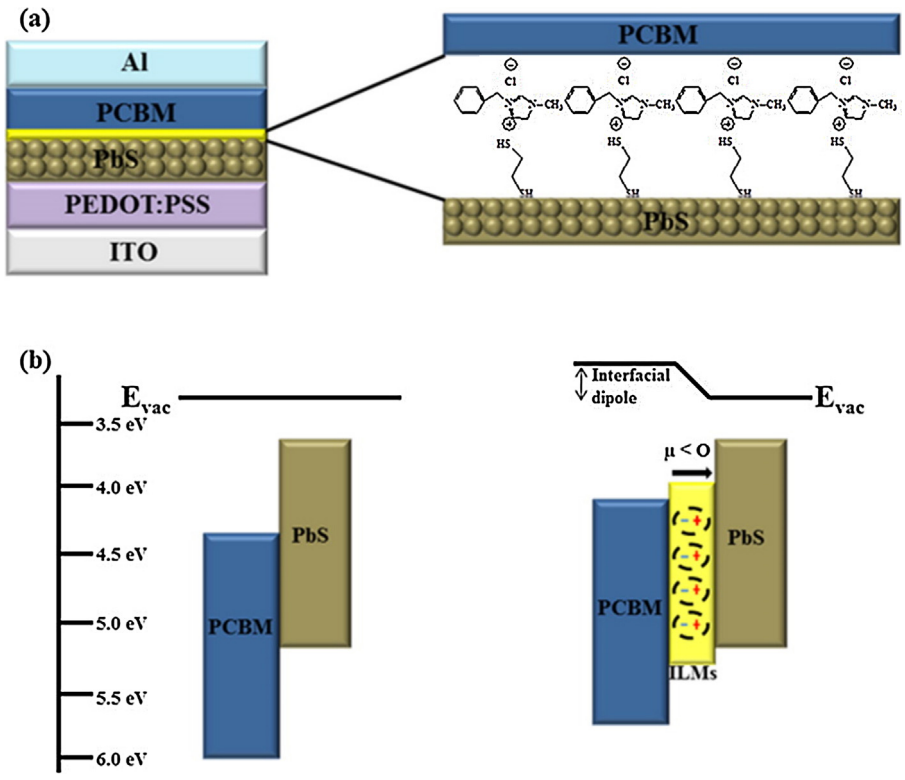

Figure 10 (a) Device architecture of PbS/PCBM hybrid quantum dot-organic solar cells with ionic liquid molecules layer. (b) Schematic energy diagrams for flat band condition without and with an ILM layer.
Reprinted with the permission from [211]. Copyrights 2013 American Chemical Society.

of these nanomaterials. Recent years have brought the less studied organic shells of QDs formed by surface ligands to the frontier of nanoscience, since this is the most versatile, labile, and processable component of any colloidal QD. Numerous published data show that surface ligands can considerably affect the photoluminescence and carrier dynamics of QDs, sometimes even exceeding the effects achieved by passivation of QD cores by inorganic shells. An almost unlimited variety of organic compounds and modern synthetic methods of organic chemistry provide a very powerful toolbox for fine tuning of QDs to their specific application niches, offering researchers and engineers the possibility to modify the emission properties of QDs or to use them as the most effective components of biotechnological and optoelectronic products.

Investigations of ligand-specific charge transfer processes in QD-based systems are of utmost importance. Modern techniques, such as transient spectroscopy and time-resolved photoluminescence measurements, along with fluorescence microscopy techniques, allow us to visualize the details of charge transfer on the single-particle and ensemble-averaged levels. Further development of instrumentation and generalized investigation techniques could make it possible to correlate the dynamic characteristics of ligands, including their position on the surface, orientation, and conformation, with the charge-transfer properties of a QD as a whole at the molecular level.

We consider the application-driven development of novel ligands by methods of combinatorial chemistry, similar to those used in drug design, to be a promising approach that will help us to control the optical and electrical responses of QDs in the future. By adapting the structure of the ligands and choosing the appropriate type of polar groups and the carbon radicals, one could switch between efficient charge carrier generation (CT ''on'') and radiative recombination (CT ''off'') in QDs, both processes with a near-unity quantum yield Specifically, this could be achieved by introducing special charge ''buffer'' (e.g., condensed aromatics), ''transfer'' (unsaturated chains) or ''blocking'' (alkane or perfluoroalkane) fragments into the structure of the carbon radical residue, which is basically responsible for QD stabilization in surrounding media. Therefore, efforts should be aimed at developing the general principles of ligand-mediated charge transfer in QD-based systems through thorough understanding of how any tiny fragment of the ligand molecule can affect the transfer properties of the whole ligand.

Acknowledgements

This work was supported by the Russian Science Foundation (grant no. 14-13-01160). We thank Vladimir Ushakov for help in the preparation of this manuscript.

References

[1] M.V. Kovalenko, L. Manna, A. Cabot, Z. Hens, D.V. Talapin, C.R. Kagan, V.I. Klimov, A.L. Rogach, P. Reiss, D.J. Milliron, P.

Guyot-Sionnnest, G. Konstantatos, W.J. Parak, T. Hyeon, B.A. Korgel, C.B. Murray, W. Heiss, ACS Nano 9 (2015) 1012—1057.
[2] D. Bera, L. Qian, T.K. Tseng, P.H. Holloway, Materials (Basel) 3 (2010) 2260—2345.
[3] S. Jun, J. Lee, E. Jang, ACS Nano 7 (2013) 1472—1477.
[4] A.G. Pattantyus-Abraham, I.J. Kramer, A.R. Barkhouse, X. Wang, G. Konstantatos, R. Debnath, L. Levina, I. Raabe, M.K. Nazeeruddin, M. Grätzel, E.H. Sargent, ACS Nano 4 (2010) 3374—3380.
[5] H.K. Jun, M.A. Careem, A.K. Arof, Renew. Sustain. Energy Rev. 22 (2013) 148—167.
[6] R. Liu, H. Huang, H. Li, Y. Liu, J. Zhong, Y. Li, S. Zhang, Z. Kang, ACS Catal. 4 (2013) 328—336.
[7] L. Amirav, A.P. Alivisatos, J. Am. Chem. Soc. 135 (2013) 13049—13053.
[8] I. Nabiev, S. Mitchell, A. Davies, Y. Williams, D. Kelleher, R. Moore, Y.K. Gun'ko, S. Byrne, Y.P. Rakovich, J.F. Donegan, A. Sukhanova, J. Conroy, D. Cottell, N. Gaponik, A. Rogach, Y. Volkov, Nano Lett. 7 (2007) 3452—3461.
[9] Y. Wang, R. Hu, G. Lin, I. Roy, K.T. Yong, ACS Appl. Mater. Interfaces 5 (2013) 2786—2799.
[10] A. Sukhanova, J. Devy, L. Venteo, H. Kaplan, M. Artemyev, V. Oleinikov, D. Klinov, M. Pluot, J.H.M. Cohen, I. Nabiev, Anal. Biochem. 324 (2004) 60—67.
[11] B. Zorman, M.V. Ramakrishna, R.A. Friesner, J. Phys. Chem. 99 (1995) 7649—7653.
[12] R. Wargnier, A.V. Baranov, V.G. Maslov, V. Stsiapura, M. Artemyev, M. Pluot, A. Sukhanova, I. Nabiev, Nano Lett. 4 (2004) 451—457.
[13] A. Rakovich, A. Sukhanova, N. Bouchonville, E. Lukashev, V. Oleinikov, M. Artemyev, V. Lesnyak, N. Gaponik, M. Molinari, M. Troyon, Y.P. Rakovich, J.F. Donegan, I. Nabiev, Nano Lett. 10 (2010) 2640—2648.
[14] V. Krivenkov, P. Samokhvalov, D. Solovyeva, R. Bilan, A. Chistyakov, I. Nabiev, Opt. Lett. 40 (2015) 1440—1443.
[15] Z. Xia, Y. Xing, M.-K. So, A.L. Koh, R. Sinclair, J. Rao, Anal. Chem. 80 (2008) 8649—8655.
[16] P. Chan, Nucleic Acids Res. 33 (2005) e161.
[17] W.C. Chan, D.J. Maxwell, X. Gao, R.E. Bailey, M. Han, S. Nie, Curr. Opin. Biotechnol. 13 (2002) 40—46.
[18] S. Saurabh, L.E. Beck, S. Maji, C.J. Baty, Y. Wang, Q. Yan, S.C. Watkins, M.P. Bruchez, ACS Nano 8 (2014) 11138—11146.
[19] S. Abe, R.K. Capek, B. De Geyter, Z. Hens, ACS Nano 7 (2013) 943—949.
[20] J. Van Embden, P. Mulvaney, Langmuir 21 (2005) 10226—10233.
[21] C.M. Evans, A.M. Love, E.A. Weiss, J. Am. Chem. Soc. 134 (2012) 17298—17305.
[22] I.C. Baek, S. Il Seok, N.C. Pramanik, S. Jana, M.A. Lim, B.Y. Ahn, C.J. Lee, Y.J. Jeong, J. Colloid Interface Sci. 310 (2007) 163—166.
[23] R. García-Rodríguez, H. Liu, J. Am. Chem. Soc. 136 (2014) 1968—1975.
[24] B. Mahler, N. Lequeux, B. Dubertret, J. Am. Chem. Soc. 132 (2010) 953—959.
[25] Y. Gao, X. Peng, J. Am. Chem. Soc. 136 (2014) 6724—6732.
[26] A.J. Morris-Cohen, M. Malicki, M.D. Peterson, J.W.J. Slavin, E.A. Weiss, Chem. Mater. 25 (2013) 1155—1165.
[27] M. Dasog, G.B. De los Reyes, L.V. Titova, F.A. Hegmann, J.G.C. Veinot, ACS Nano 8 (2014) 9636—9648.
[28] I.-S. Liu, H.-H. Lo, C.-T. Chien, Y.-Y. Lin, C.-W. Chen, Y.-F. Chen, W.-F. Su, S.-C. Liou, J. Mater. Chem. 18 (2008) 675—682.
[29] S.F. Wuister, C. De Mello Donegá, A. Meijerink, J. Phys. Chem. B 108 (2004) 17393—17397.
[30] D.V. Talapin, A.L. Rogach, A. Kornowski, M. Haase, H. Weller, Nano Lett. 1 (2001) 207—211.
[31] B. Fitzmorris, Y. Pu, J. Cooper, Appl. Mater. Interfaces 5 (2013) 2893—2900.
[32] P. Samokhvalov, M. Artemyev, I. Nabiev, Chem. Eur. J. 19 (2013) 1534—1546.
[33] P. Samokhvalov, P. Linkov, J. Michel, M. Molinari, I. Nabiev, in: X. Zhang, H. Ming, C. Yu (Eds.), Proc. SPIE, vol. 8955, 2014, 89550S(1)—89550S(6).
[34] K. Boldt, N. Kirkwood, G.A. Beane, P. Mulvaney, Chem. Mater. 25 (2013) 4731—4738.
[35] S. Jun, E. Jang, Angew. Chem. Int. Ed. 52 (2013) 679—682.
[36] O. Chen, J. Zhao, V.P. Chauhan, J. Cui, C. Wong, D.K. Harris, H. Wei, H.-S. Han, D. Fukumura, R.K. Jain, M.G. Bawendi, Nat. Mater. 12 (2013) 445—451.
[37] Y. Zhang, A. Clapp, Sensors 11 (2011) 11036—11055.
[38] C. Radhakrishnan, M.K.F. Lo, C.M. Knobler, M.A. Garcia-Garibay, H.G. Monbouquette, Langmuir 27 (2011) 2099—2103.
[39] H. Zhu, M.Z. Hu, L. Shao, K. Yu, R. Dabestani, M.B. Zaman, S. Liao, J. Nanomater. 2014 (2014).
[40] E. Zillner, S. Fengler, P. Niyamakom, F. Rauscher, K. Köhler, T. Dittrich, J. Phys. Chem. C 116 (2012) 16747—16754.
[41] R.A. Marcus, N. Sutin, Biochim. Biophys. Acta — Rev. Bioenergy 811 (1985) 265—322.
[42] J.H. Bang, P.V. Kamat, ACS Nano 5 (2011) 9421—9427.
[43] A. Pal, S. Srivastava, R. Gupta, S. Sapra, Phys. Chem. Chem. Phys. 15 (2013) 15888—15895.
[44] J. Jasieniak, M. Califano, S.E. Watkins, ACS Nano 5 (2011) 5888—5902.
[45] B.P. Bloom, L. Bin Zhao, Y. Wang, D.H. Waldeck, R. Liu, P. Zhang, D.N. Beratan, J. Phys. Chem. C 117 (2013) 22401—22411.
[46] C. Querner, P. Reiss, S. Sadki, M. Zagorska, A. Pron, Phys. Chem. Chem. Phys. 7 (2005) 3204—3209.
[47] S.N. Inamdar, P.P. Ingole, S.K. Haram, ChemPhysChem 9 (2008) 2574—2579.
[48] A.M. Munro, B. Zacher, A. Graham, N.R. Armstrong, ACS Appl. Mater. Interfaces 2 (2010) 863—869.
[49] A.E. Kuznetsov, D.N. Beratan, J. Phys. Chem. C 118 (2014) 7094—7109.
[50] Z. Zhang, D. Li, R. Xie, W. Yang, Angew. Chem. Int. Ed. 52 (2013) 5052—5055.
[51] S.K. Haram, A. Kshirsagar, Y.D. Gujarathi, P.P. Ingole, O.A. Nene, G.B. Markad, S.P. Nanavati, J. Phys. Chem. C 115 (2011) 6243—6249.
[52] T.J. Jacobsson, T. Edvinsson, J. Phys. Chem. C 118 (2014) 12061—12072.
[53] M. Scheele, D. Hanifi, D. Zherebetskyy, S.T. Chourou, S. Axnanda, B.J. Rancatore, K. Thorkelsson, T. Xu, Z. Liu, L.W. Wang, Y. Liu, A.P. Alivisatos, ACS Nano 8 (2014) 2532—2540.
[54] M. Soreni-Harari, N. Yaacobi-Gross, D. Steiner, A. Aharoni, U. Banin, O. Millo, N. Tessler, Nano Lett. 8 (2008) 678—684.
[55] J. Sun, J. Zhao, Y. Masumoto, Appl. Phys. Lett. 102 (2013) 053119.
[56] Z. Zhou, J. Shi, P. Wu, M. Li, L. Guo, Chem. Phys. Lett. 513 (2011) 72—76.
[57] C. Safa, P. Kasap, Handbook of Electronic and Photonic Materials, Springer, 2007.
[58] R. Ferro, J. Rodrıíguez, Sol. Energy Mater. Sol. Cells 64 (2000) 363—370.
[59] Y. Dou, T. Fishlock, R.G. Egdell, D.S.L. Law, G. Beamson, Phys. Rev. B 55 (1997) R13381—R13384.
[60] E.M. Miller, Y. Zhao, C.C. Mercado, S.K. Saha, J.M. Luther, K. Zhu, V. Stevanović, C.L. Perkins, J. van de Lagemaat, Phys. Chem. Chem. Phys. 16 (2014) 22122—22130.
[61] T. Baikie, Y. Fang, J.M. Kadro, M. Schreyer, F. Wei, S.G. Mhaisalkar, M. Graetzel, T.J. White, J. Mater. Chem. A 1 (2013) 5628—5641.
[62] R. Comin, G. Walters, E.S. Thibau, O. Voznyy, Z.-H. Lu, E.H. Sargent, J. Mater. Chem. C 3 (2015) 8839—8843.
[63] S.A. Fischer, A.M. Crotty, S.V. Kilina, S.A. Ivanov, S. Tretiak, Nanoscale 4 (2012) 904—914.

[64] C.-F. Chi, H.-W. Cho, H. Teng, C.-Y. Chuang, Y.-M. Chang, Y.-J. Hsu, Y.-L. Lee, Appl. Phys. Lett. 98 (2011) 012101.
[65] X. Chen, J. Vac. Sci. Technol. B: Microelectron. Nanometer. Struct. 13 (1995) 1715—1727.
[66] F. García-Santamaría, Y. Chen, J. Vela, R.D. Schaller, J.A. Hollingsworth, V.I. Klimov, Nano Lett. 9 (2009) 3482—3488.
[67] B. Carlson, K. Leschkies, E.S. Aydil, X.Y. Zhu, J. Phys. Chem. C 112 (2008) 8419—8423.
[68] R. Li, C. Cai, L. Hu, H. Wu, W. Zhang, J. Zhu, Appl. Surf. Sci. 276 (2013) 258—261.
[69] X. Ma, A. Mews, T. Kipp, J. Phys. Chem. C 117 (2013) 16698—16708.
[70] A.L. Devine, M.G.D. Nix, R.N. Dixon, M.N.R. Ashfold, J. Phys. Chem. A 112 (2008) 9563—9574.
[71] Z. Ning, M. Molnár, Y. Chen, P. Friberg, L. Gan, H. Ågren, Y. Fu, Phys. Chem. Chem. Phys. 13 (2011) 5848—5854.
[72] D.H. Aue, H.M. Webb, M.T. Bowers, J. Am. Chem. Soc. 98 (1976) 311—317.
[73] M.T.G. Marco Montalti, A. Credi, L. Prodi, Handb Photochem, third ed., CRC Press, 2006, pp. 493—527.
[74] P.J. Linstrom, W.G. Mallard, NIST WebBook, National Institute of Standards and Technology, Gaithersburg, MD, 2010.
[75] T. Virgili, A. Calzolari, I. Suárez López, B. Vercelli, G. Zotti, A. Catellani, A. Ruini, F. Tassone, J. Phys. Chem. C 117 (2013) 5969—5974.
[76] J. Huang, Z. Huang, Y. Yang, H. Zhu, T. Lian, J. Am. Chem. Soc. 132 (2010) 4858—4864.
[77] H. Zhu, Y. Yang, K. Hyeon-Deuk, M. Califano, N. Song, Y. Wang, W. Zhang, O.V. Prezhdo, T. Lian, Nano Lett. 14 (2014) 1263—1269.
[78] A. Boulesbaa, A. Issac, D. Stockwell, Z. Huang, J. Huang, J. Guo, T. Lian, J. Am. Chem. Soc. 129 (2007) 15132—15133.
[79] A. Boulesbaa, Z. Huang, D. Wu, T. Lian, J. Phys. Chem. C 114 (2010) 962—969.
[80] A. Issac, S. Jin, T. Lian, J. Am. Chem. Soc. 130 (2008) 11280—11281.
[81] S. Jagadeeswari, M. Asha Jhonsi, A. Kathiravan, R. Renganathan, J. Lumin. 131 (2011) 597—602.
[82] A.J. Morris-Cohen, M.T. Frederick, L.C. Cass, A.E. Weiss, J. Am. Chem. Soc. 133 (2011) 10146—10154.
[83] L. Dworak, V.V. Matylitsky, V.V. Breus, M. Braun, T. Basché, J. Wachtveitl, J. Phys. Chem. C 115 (2011) 3949—3955.
[84] M. Tagliazucchi, D.B. Tice, C.M. Sweeney, A.J. Morris-Cohen, E.A. Weiss, ACS Nano 5 (2011) 9907—9917.
[85] A.J. Morris-Cohen, M.D. Peterson, M.T. Frederick, J.M. Kamm, E.A. Weiss, J. Phys. Chem. Lett. 3 (2012) 2840—2844.
[86] T. Uematsu, A. Doko, T. Torimoto, K. Oohora, T. Hayashi, S. Kuwabata, J. Phys. Chem. C 117 (2013) 15667—15676.
[87] Y.B. Lou, X.B. Chen, A.C. Samia, C. Burda, J. Phys. Chem. B 107 (2003) 12431—12437.
[88] K.E. Knowles, M. Malicki, E.A. Weiss, J. Am. Chem. Soc. 134 (2012) 12470—12473.
[89] M.D. Peterson, R.J. Holbrook, T.J. Meade, E.A. Weiss, J. Am. Chem. Soc. 135 (2013) 13162—13167.
[90] J. Huang, D. Stockwell, Z. Huang, D.L. Mohler, T. Lian, J. Am. Chem. Soc. 130 (2008) 5632—5633.
[91] A.M. Scott, W.R. Algar, M.H. Stewart, S.A. Trammell, J.B. Blanco-Canosa, P.E. Dawson, J.R. Deschamps, R. Goswami, E. Oh, A.L. Huston, I.L. Medintz, J. Phys. Chem. C 118 (2014) 9239—9250.
[92] S.A. Gallagher, S. Comby, M. Wojdyla, T. Gunnlaugsson, J.M. Kelly, Y.K. Gun'Ko, I.P. Clark, G.M. Greetham, M. Towrie, S.J. Quinn, Inorg. Chem. 52 (2013) 4133—4135.
[93] J. Huang, K.L. Mulfort, P. Du, L.X. Chen, J. Am. Chem. Soc. 134 (2012) 16472—16475.
[94] M.H. Stewart, A.L. Huston, A.M. Scott, E. Oh, W.R. Algar, J.R. Deschamps, K. Susumu, V. Jain, D.E. Prasuhn, J. Blanco-canosa, P.E. Dawson, I.L. Medintz, ACS Nano (2013) 9489—9505.
[95] V.V. Chaban, V.V. Prezhdo, O.V. Prezhdo, J. Phys. Chem. Lett. 4 (2013) 1—6.
[96] N. Song, H. Zhu, S. Jin, W. Zhan, T. Lian, ACS Nano 5 (2011) 613—621.
[97] S.C. Cui, T. Tachikawa, M. Fujitsuka, T. Majima, J. Phys. Chem. C 115 (2011) 1824—1830.
[98] F. Mammeri, A. Ballarin, M. Giraud, G. Brusatin, S. Ammar, Colloids Surf. A: Physicochem. Eng. Asp. 439 (2013) 138—144.
[99] A.J. Nozik, Annu. Rev. Phys. Chem. 52 (2001) 193—231.
[100] Y. Yang, W. Rodríguez-Córdoba, T. Lian, Nano Lett. 12 (2012) 4235—4241.
[101] X. Qu, J.B. Chaires, J. Am. Chem. Soc. 123 (2001) 1—7.
[102] S.-C. Cui, T. Tachikawa, M. Fujitsuka, T. Majima, J. Phys. Chem. C 112 (2008) 19625—19634.
[103] M.A. Jhonsi, R. Renganathan, J. Colloid Interface Sci. 344 (2010) 596—602.
[104] S. Impellizzeri, B. McCaughan, J.F. Callan, F.M. Raymo, J. Am. Chem. Soc. 134 (2012) 2276—2283.
[105] K.E. Knowles, D.B. Tice, E.A. McArthur, G.C. Solomon, E.A. Weiss, J. Am. Chem. Soc. 132 (2010) 1041—1050.
[106] J. Bang, J. Park, R. Velu, E. Yoon, K. Lee, S. Cho, S. Cha, G. Chae, T. Joo, S. Kim, Chem. Commun. 48 (2012) 9174—9176.
[107] S. Sadhu, M. Tachiya, A. Patra, J. Phys. Chem. C 113 (2009) 19488—19492.
[108] J. Huang, Z. Huang, S. Jin, T. Lian, J. Phys. Chem. C 112 (2008) 19734—19738.
[109] M.D. Porter, T.B. Bright, D.L. Allara, C.E.D. Chidsey, JACS 109 (1987) 3559—3568.
[110] D. Grumelli, L.P. Méndez De Leo, C. Bonazzola, V. Zamlynny, E.J. Calvo, R.C. Salvarezza, Langmuir 26 (2010) 8226—8232.
[111] M.J. Hostetler, J.J. Stokes, R.W. Murray, Langmuir 12 (1996) 3604—3612.
[112] M. Wu, P. Mukherjee, D.N. Lamont, D.H. Waldeck, J. Phys. Chem. 114 (2010) 5751—5759.
[113] S.-C. Cui, T. Tachikawa, M. Fujitsuka, T. Majima, J. Phys. Chem. C 114 (2010) 1217—1225.
[114] J. Tang, R.A. Marcus, Phys. Rev. Lett. 95 (2005), 1071401(1)—107401(4).
[115] J.L. Ellis, D.D. Hickstein, K.J. Schnitzenbaumer, M.B. Wilker, B.B. Palm, J.L. Jimenez, G. Dukovic, H.C. Kapteyn, M.M. Murnane, W. Xiong, J. Am. Chem. Soc. 137 (2015) 3759—3762.
[116] C. Landes, C. Burda, M. Braun, M.A. El-Sayed, J. Phys. Chem. B 105 (2001) 2981—2986.
[117] S.N. Sharma, Z.S. Pillai, P.V. Kamat, J. Phys. Chem. B 107 (2003) 10088—10093.
[118] Z. Xu, C.R. Hine, M.M. Maye, Q. Meng, M. Cotlet, ACS Nano 6 (2012) 4984—4992.
[119] Z. Youlin, J. Pengtao, Z. Qinghui, S. Yajuan, S. Huaipeng, Y.A. Wang, K. Xianggui, Z. Jialong, Z. Hong, J. Phys. Chem. C 113 (2009) 1886—1890.
[120] P. Singhal, H.N. Ghosh, J. Phys. Chem. C 118 (2014) 16358—16365.
[121] M. Malicki, K.E. Knowles, E.A. Weiss, Chem. Commun. 49 (2013) 4400—4402.
[122] N. Song, H. Zhu, S. Jin, T. Lian, ACS Nano 5 (2011) 8750—8759.
[123] S. Brovelli, C. Galland, R. Viswanatha, V.I. Klimov, Nano Lett. 12 (2012) 4372—4379.
[124] A. Avidan, I. Pinkas, D. Oron, ACS Nano 6 (2012) 3063—3069.
[125] H.H. Wei, C. Evans, A. Neukirch, J. Young, O.V. Prezhdo, T.D. Krauss, Nano Lett. (2012) 4465—4471.
[126] M. Abdellah, K.J. Karki, N. Lenngren, K. Zheng, T. Pascher, A. Yartsev, T. Pullerits, J. Phys. Chem. C 118 (2014) 21682—21686.
[127] M.B. Teunis, S. Dolai, R. Sardar, Langmuir 30 (2014) 7851—7858.

[128] B.K. Hughes, D.A. Ruddy, J.L. Blackburn, D.K. Smith, M.R. Bergren, A.J. Nozik, J.C. Johnson, M.C. Beard, ACS Nano 6 (2012) 5498—5506.
[129] M. Abdellah, R. Marschan, K. Zidek, M.E. Messing, A. Abdelwahab, P. Chabera, K. Zheng, T. Pullerits, J. Phys. Chem. C 118 (2014) 25802—25808.
[130] B. Omogo, J.F. Aldana, C.D. Heyes, J. Phys. Chem. C 117 (2013) 2317—2327.
[131] J.J. Li, Y.A. Wang, W. Guo, J.C. Keay, T.D. Mishima, M.B. Johnson, X. Peng, J. Am. Chem. Soc. 125 (2003) 12567—12575.
[132] W.K. Bae, J. Joo, L.A. Padilha, J. Won, D.C. Lee, Q. Lin, W. Koh, H. Luo, V.I. Klimov, J.M. Pietryga, J. Am. Chem. Soc. 134 (2012) 20160—20168.
[133] R.C. Page, D. Espinobarro-Velazquez, M.A. Leontiadou, C. Smith, E.A. Lewis, S.J. Haigh, C. Li, H. Radtke, A. Pengpad, F. Bondino, E. Magnano, I. Pis, W.R. Flavell, P. O'Brien, D.J. Binks, Small 11 (2015) 1548—1554.
[134] Z. Ning, Y. Ren, S. Hoogland, O. Voznyy, L. Levina, P. Stadler, X. Lan, D. Zhitomirsky, E.H. Sargent, Adv. Mater. 24 (2012) 6295—6299.
[135] J.D. Rinehart, A.M. Schimpf, A.L. Weaver, A.W. Cohn, D.R. Gamelin, J. Am. Chem. Soc. 135 (2013) 18782—18785.
[136] T.X. Ding, J.H. Olshansky, S.R. Leone, A.P. Alivisatos, J. Am. Chem. Soc. 137 (2015) 2021—2029.
[137] W.-T. Sun, Y. Yu, H.-Y. Pan, X.-F. Gao, Q. Chen, L.-M. Peng, J. Am. Chem. Soc. 130 (2008) 1124—1125.
[138] L. Pan, J.-J. Zou, S. Wang, Z.-F. Huang, A. Yu, L. Wang, X. Zhang, Chem. Commun. (Camb.) 49 (2013) 6593—6595.
[139] Y. Zhang, T. Xie, T. Jiang, X. Wei, S. Pang, X. Wang, D. Wang, Nanotechnology 20 (2009) 155707.
[140] G. Wang, X. Yang, F. Qian, J.Z. Zhang, Y. Li, Nano Lett. 10 (2010) 1088—1092.
[141] K.S. Leschkies, R. Divakar, J. Basu, E. Enache-Pommer, J.E. Boercker, C.B. Carter, U.R. Kortshagen, D.J. Norris, E.S. Aydil, Nano Lett. 7 (2007) 1793—1798.
[142] L. Jiang, G. Sun, Z. Zhou, S. Sun, Q. Wang, S. Yan, H. Li, J. Tian, J. Guo, B. Zhou, Q. Xin, J. Phys. Chem. B 109 (2005) 8774—8778.
[143] M. Aziz, S. Saber Abbas, W.R. Wan Baharom, Mater. Lett. 91 (2013) 31—34.
[144] H.N. Lim, R. Nurzulaikha, I. Harrison, S.S. Lim, W.T. Tan, M.C. Yeo, M.A. Yarmo, N.M. Huang, Ceram. Int. 38 (2012) 4209—4216.
[145] X. Wang, G. Liu, Z.-G. Chen, F. Li, L. Wang, G.Q. Lu, H.-M. Cheng, Chem. Commun. (2009) 3452—3454.
[146] J. Zhao, M.A. Holmes, F.E. Osterloh, ACS Nano 7 (2013) 4316—4325.
[147] Y. Li, J.Z. Zhang, Laser Photon. Rev. 4 (2009) 517—528.
[148] X. Wang, G. Liu, G.Q. Lu, H.-M. Cheng, Int. J. Hydrogen Energy 35 (2010) 8199—8205.
[149] Z. Tachan, I. Hod, M. Shalom, L. Grinis, A. Zaban, Phys. Chem. Chem. Phys. 15 (2013) 3841—3845.
[150] K. Prabakar, S. Minkyu, S. Inyoung, K. Heeje, J. Phys. D: Appl. Phys. 43 (2009) 012002.
[151] P. Kundu, P.A. Deshpande, G. Madras, N. Ravishankar, J. Mater. Chem. 21 (2011) 4209—4216.
[152] M.A. Hossain, J.R. Jennings, Z.Y. Koh, Q. Wang, ACS Nano 5 (2011) 3172—3181.
[153] D. Wang, H. Zhao, N. Wu, M.A. El Khakani, D. Ma, J. Phys. Chem. Lett. 1 (2010) 1030—1035.
[154] I. Robel, M. Kuno, P.V. Kamat, J. Am. Chem. Soc. 129 (2007) 4136—4137.
[155] M.H. Dean, U. Stimming, J. Electroanal. Chem. Interfacial Electrochem. 228 (1987) 135—151.
[156] V. Chakrapani, K. Tvrdy, P.V. Kamat, J. Am. Chem. Soc. 132 (2010) 1228—1229.
[157] H. Choi, P.K. Santra, V.P. Kamat, ACS Nano 6 (2012) 5718—5726.
[158] J.S. Nevins, K.M. Coughlin, D.F. Watson, ACS Appl. Mater. Interfaces 3 (2011) 4242—4253.
[159] K.M. Coughlin, J.S. Nevins, D.F. Watson, ACS Appl. Mater. Interfaces 5 (2013) 8649—8654.
[160] H.J. Yun, T. Paik, M.E. Edley, J.B. Baxter, C.B. Murray, ACS Appl. Mater. Interfaces 6 (2014) 3721—3728.
[161] H. Wang, E.R. McNellis, S. Kinge, M. Bonn, E. Cánovas, Nano Lett. 13 (2013) 5311—5315.
[162] T. Hansen, K. Zheng, M. Abdellah, P. Persson, J. Phys. Chem. Lett. 5 (2014) 1157—1162.
[163] M.A. Ratner, J. Phys. Chem. 94 (1990) 4877—4883.
[164] D.A. Hines, P.V. Kamat, J. Phys. Chem. C 117 (2013) 14418—14426.
[165] M.T. Frederick, V.A. Amin, N.K. Swenson, A.Y. Ho, E.A. Weiss, Nano Lett. 13 (2013) 287—292.
[166] P.K. Santra, P.V. Nair, K. George Thomas, P.V. Kamat, C. Sensitized, Q. Dot, S. Cell, E. Dynamics, P. Performance, J. Phys. Chem. Lett. 4 (2013) 722—729.
[167] M. Abdellah, K. Žídek, K. Zheng, P. Chábera, M.E. Messing, T. Pullerits, J. Phys. Chem. Lett. 4 (2013) 1760—1765.
[168] M. Sun, D. Zhu, W. Ji, P. Jing, X. Wang, W. Xiang, J. Zhao, ACS Appl. Mater. Interfaces 5 (2013) 12681—12688.
[169] D.G. Sellers, D.F. Watson, J. Phys. Chem. C 116 (2012) 19215—19224.
[170] J. Han, L. Wang, S.S. Wong, J. Phys. Chem. C 118 (2014) 5671—5682.
[171] M. Ni, M.K.H. Leung, D.Y.C. Leung, K. Sumathy, Renew. Sustain. Energy Rev. 11 (2007) 401—425.
[172] A. Kudo, Y. Miseki, Chem. Soc. Rev. 38 (2009) 253—278.
[173] G. Palmisano, V. Augugliaro, M. Pagliaro, L. Palmisano, Chem. Commun. (2007) 3425—3437.
[174] M. D'Auria, L. Emanuele, R. Racioppi, V. Velluzzi, J. Hazard. Mater. 164 (2009) 32—38.
[175] J. Grzechulska, Water Res. 34 (2000) 1638—1644.
[176] R.J. Berry, M.R. Mueller, Microchem. J. 50 (1994) 28—32.
[177] M. Pidou, S.A. Parsons, G. Raymond, P. Jeffrey, T. Stephenson, B. Jefferson, Water Res. 43 (2009) 3932—3939.
[178] A. Whelan, F. Regan, J. Environ. Monit. 8 (2006) 880—886.
[179] K. Hashimoto, H. Irie, A. Fujishima, Jpn. J. Appl. Phys. 44 (2005) 8269—8285.
[180] Y. Xie, G. Ali, S.H. Yoo, S.O. Cho, ACS Appl. Mater. Interfaces 2 (2010) 2910—2914.
[181] N. Daneshvar, D. Salari, A. Khataee, J. Photochem. Photobiol. A: Chem. 162 (2004) 317—322.
[182] S. Chakrabarti, B. Dutta, J. Hazard. Mater. 112 (2004) 269—278.
[183] H. Zhu, N. Song, H. Lv, C.L. Hill, T. Lian, J. Am. Chem. Soc. 134 (2012) 11701—11708.
[184] C. Ratanatawanate, Y. Tao, K.J. Balkus, J. Phys. Chem. C 113 (2009) 10755—10760.
[185] G.-S. Li, D.-Q. Zhang, J.C. Yu, Environ. Sci. Technol. (2009) 7079—7085.
[186] J. Hensel, G. Wang, Y. Li, J.Z. Zhang, Nano Lett. 10 (2010) 478—483.
[187] C.M. Chang, K.L. Orchard, B.C.M. Martindale, E. Reisner, J. Mater. Chem. A (2015) 1—8.
[188] M.F. Kuehnel, D.W. Wakerley, K.L. Orchard, E. Reisner, Angew. Chem. Int. Ed. 54 (2015) 9627—9631.
[189] C.M. Bernt, P.T. Burks, A.W. Demartino, A.E. Pierri, E.S. Levy, D.F. Zigler, P.C. Ford, J. Am. Chem. Soc. 136 (2014) 2192—2195.
[190] C. Pak, J.Y. Woo, K. Lee, W.D. Kim, Y. Yoo, D.C. Lee, J. Phys. Chem. C 116 (2012) 25407—25414.
[191] K.P. Acharya, R.S. Khnayzer, T. O'Connor, G. Diederich, M. Kirsanova, A. Klinkova, D. Roth, E. Kinder, M. Imboden, M. Zamkov, Nano Lett. 11 (2011) 2919—2926.

[192] A. Thibert, F.A. Frame, E. Busby, M.A. Holmes, F.E. Osterloh, D.S. Larsen, J. Phys. Chem. Lett. 2 (2011) 2688—2694.
[193] C. Ratanatawanate, A. Bui, K. Vu, K.J. Balkus, J. Phys. Chem. C 115 (2011) 6175—6180.
[194] Z. Kang, C.H.A. Tsang, N.-B. Wong, Z. Zhang, S.-T. Lee, J. Am. Chem. Soc. 129 (2007) 12090—12091.
[195] J. Kwak, W.K. Bae, D. Lee, I. Park, J. Lim, M. Park, H. Cho, H. Woo, D.Y. Yoon, K. Char, S. Lee, C. Lee, Nano Lett. 12 (2012) 2362—2366.
[196] D.P. Puzzo, E.J. Henderson, M.G. Helander, Z. Wang, G.A. Ozin, Z. Lu, Nano Lett. 11 (2011) 1585—1590.
[197] S. Bhaumik, A.J. Pal, ACS Appl. Mater. Interfaces 6 (2014) 11348—11356.
[198] H. Shen, Q. Lin, H. Wang, L. Qian, Y. Yang, A. Titov, J. Hyvonen, Y. Zheng, L.S. Li, ACS Appl. Mater. Interfaces 5 (2013) 12011—12016.
[199] A. Castan, H.-M. Kim, J. Jang, ACS Appl. Mater. Interfaces 6 (2014) 2508—2515.
[200] M.D. Ho, D. Kim, N. Kim, S.M. Cho, H. Chae, ACS Appl. Mater. Interfaces 5 (2013) 12369—12374.
[201] W. Ji, Y. Tian, Q. Zeng, S. Qu, L. Zhang, P. Jing, J. Wang, J. Zhao, ACS Appl. Mater. Interfaces (2014) 14001—14007.
[202] S. Dayneko, D. Lypenko, P. Linkov, A. Tameev, I. Martynov, P. Samokhvalov, A. Chistyakov, in: X. Zhang, H. Ming, C. Yu (Eds.), Proc. SPIE, vol. 9270, 2014, 927009(1)—927009(6).
[203] S. Bhaumik, A.J. Pal, J. Phys. Chem. C 117 (2013) 25390—25396.
[204] M. Zorn, W.K. Bae, J. Kwak, H. Lee, C. Lee, R. Zentel, K. Char, ACS Nano 3 (2009) 1063—1068.
[205] I. Hod, A. Zaban, Langmuir 30 (2014) 7264—7273.
[206] I. Robel, V. Subramanian, M. Kuno, P.V. Kamat, J. Am. Chem. Soc. 128 (2006) 2385—2393.
[207] C.-H.M. Chuang, P.R. Brown, V. Bulović, M.G. Bawendi, Nat. Mater. 13 (2014) 796—801.
[208] B. Ehrler, K.P. Musselman, M.L. Böhm, F.S.F. Morgenstern, Y. Vaynzof, B.J. Walker, J.L. Macmanus-Driscoll, N.C. Greenham, ACS Nano 7 (2013) 4210—4220.
[209] S.H. Park, A. Roy, S. Beaupré, S. Cho, N. Coates, J.S. Moon, D. Moses, M. Leclerc, K. Lee, A.J. Heeger, Nat. Photonics 3 (2009) 297—302.
[210] P. Peumans, S. Uchida, S.R. Forrest, Nature 425 (2003) 158—162.
[211] G.-H. Kim, H.-B. Kim, B. Walker, H. Choi, C. Yang, J. Park, J.Y. Kim, ACS Appl. Mater. Interfaces 5 (2013) 1757—1760.
[212] A.A. Shemetov, I. Nabiev, A. Sukhanova, ACS Nano 6 (2012) 4585—4602.
[213] C. Kirchner, T. Liedl, S. Kudera, T. Pellegrino, A. Muñoz Javier, H.E. Gaub, S. Stölzle, N. Fertig, W.J. Parak, Nano Lett. 5 (2005) 331—338.

Kirill V. Vokhmintcev, PhD, was born in 1988 in Vologda, Russia. He received his PhD degree in Chemistry, in early 2015, from the Mendeleev Russian University of Chemical Technology. His actual research in the Laboratory of Nano-Bioengineering of National Research Nuclear University MEPhI (Moscow Engineering Physics Institute), under direction of Professor Igor Nabiev, is related to the synthesis and functionalization of $A^{II}B^{VI}$ semiconductor quantum dots and their applications in optoelectronics and biomedicine. Dr. Vokhmintcev participates, as a co-PI, in the International collaborative projects involving Université de Reims Champagne-Ardenne (France), Max-Planck Institute for Experimental Medicine (Goettingen, Germany) and Institute of Electrochemistry of Russian Academy of Science, Moscow.

Dr. Pavel S. Samokhvalov was born in Arzamas-16 (Soviet Union). He received his Ph.D. degree in Chemistry from Moscow State University (Russia) in 2010. His research in the Nanochemistry Group of the Laboratory of Nano-Bioengineering of Moscow Engineering Physics Institute is related to the structural engineering, synthesis and functionalization of $A^{II}B^{VI}$ semiconductor fluorescent nanomaterials with the goal to make them adaptable to biological applications.

Igor Nabiev received his Ph.D. degree in Physics and Mathematics in 1983 from Moscow State University and his D.Sci. degree in Chemistry from the Shemyakin Institute of Bioorganic Chemistry of the Russian Academy of Sciences. After professorships in the USA and France, he was nominated as Professor of Biophysics in the University of Reims Champagne-Ardenne, France. In 2008—2009 Prof. Nabiev was a recipient of the Walton Award from the Science Foundation of Ireland. Since 2010 he has been Director of Technological Platform Semiconductor Nanocrystals of the ''Large'' European Project NAMDIATREAM awarded as the best of all the over 1000 projects launched under the EU Funding Instruments in the field of nanotechnologies and advanced materials. In 2011, Prof. Nabiev received a MEGA-grant Award in the framework of the Program of Attraction of the World Leading Scientists to Russian Institutions of Higher Education and founded the Laboratory of Nano-Bioengineering in Moscow Engineering Physics Institute.